The Transition-Zone Water Filter Model for Global Material Circulation: Where Do We Stand?

Shun-ichiro Karato, David Bercovici, Garrett Leahy,
Guillaume Richard and Zhicheng Jing

Yale University, Department of Geology and Geophysics, New Haven, CT 06520

Materials circulation in Earth's mantle will be modified if partial melting occurs in the transition zone. Melting in the transition zone is plausible if a significant amount of incompatible components is present in Earth's mantle. We review the experimental data on melting and melt density and conclude that melting is likely under a broad range of conditions, although conditions for dense melt are more limited. Current geochemical models of Earth suggest the presence of relatively dense incompatible components such as K_2O and we conclude that a dense melt is likely formed when the fraction of water is small. Models have been developed to understand the structure of a melt layer and the circulation of melt and volatiles. The model suggests a relatively thin melt-rich layer that can be entrained by downwelling current to maintain "steady-state" structure. If deep mantle melting occurs with a small melt fraction, highly incompatible elements including hydrogen, helium and argon are sequestered without much effect on more compatible elements. This provides a natural explanation for many paradoxes including (i) the apparent discrepancy between whole mantle convection suggested from geophysical observations and the presence of long-lived large reservoirs suggested by geochemical observations, (ii) the helium/heat flow paradox and (iii) the argon paradox. Geophysical observations are reviewed including electrical conductivity and anomalies in seismic wave velocities to test the model and some future directions to refine the model are discussed.

1. INTRODUCTION

The most well-known on-going chemical differentiation process on Earth is partial melting beneath mid-ocean ridges, which is primarily due to the adiabatic upwelling (*pressure-release melting*) and creates relatively "enriched" oceanic crust and "depleted" residual mantle (e.g., [*Hofmann*, 1997]). If this is the only chemical differentiation process operating at present and in the recent past, then several immediate consequences follow. For example, if one accepts the model of whole mantle convection, as suggested by seismic tomography ([*Grand*, 1994; *van der Hilst, et al.*, 1997]), then the whole mantle is depleted with only a small volume (~10%) of relatively enriched material continuously replenished by subduction of oceanic crust and sediments. This view is inconsistent with geochemical observations that suggest the entire lower mantle (~70% of the mantle) is relatively enriched [*Albarède and van der Hilst*, 2002; *Allègre, et al.*, 1996]). An alternative model assumes that differentiation at mid-ocean ridges involves material only from the upper mantle (e.g., [*Allègre, et al.*, 1996]). In this model, the deeper mantle is not involved in chemical differentiation at mid-ocean ridges and maintains relatively enriched chemical composition. However, this latter model implies strongly

Earth's Deep Water Cycle
Geophysical Monograph Series 168

10.1029/168GM22

layered convection that is not consistent with the results of seismic tomography.

High-pressure experimental studies on properties of minerals suggest that melting may not be limited to the shallow upper mantle, but may occur in the deep upper mantle or the transition-zone (e.g., [*Dasgupta and Hirschmann*, 2006; *Gasparik*, 1993; *Ohtani, et al.*, 2001; *Wang and Takahashi*, 2000; *Young, et al.*, 1993]). *P-T* conditions in the deep mantle are well below the solidus of dry, depleted peridotite so melting under deep mantle conditions would require the addition of "impurities" such as water (*flux melting*). For example, a large contrast in the solubility of water (hydrogen) between minerals in the upper mantle and the transition-zone minerals (e.g., [*Kohlstedt, et al.*, 1996]) could lead to partial melting when the upwelling materials passes the 410-km boundary. [*Bercovici and Karato*, 2003] analyzed possible consequence of this transition-zone melting on the geochemical cycling and mantle convection. They proposed that if the melt produced there is denser than the upper mantle minerals (but lighter than the transition zone minerals) then the melt will remove much of the highly incompatible elements so that the mantle will be chemically layered in terms of highly incompatible elements although the majority of mantle materials undergo the whole mantle wide convection. This transition-zone water filter model (hereafter referred to as the TZWF model) assumes the following processes: (1) The global flow pattern in Earth's mantle is dominated by the slab-related localized downwelling currents and diffuse upwelling flow forced by the slab flux that occurs more-or-less homogeneously in most of the mantle. (2) There is enough water in the transition-zone to cause dehydration-induced partial melting of ambient upwelling material as it goes to from wadsleyite-dominated assemblage to an olivine-dominated one upon crossing the 410-km boundary. (3) The melt formed there is denser than the surrounding materials in the upper mantle but lighter than the transition-zone materials and hence will be trapped at the 410 km discontinuity. (4) Partial melting removes some of the incompatible elements from the original materials and hence the residual materials are depleted with these elements. (5) The residual materials continue upwelling into the upper mantle and become the relatively depleted source materials for MORB. (6) The separation of incompatible elements (filtering) is not effective for hot plumes because hot melts have low density, high ascent velocities, and thus shorter residence times in the transition zone resulting in an "unfiltered" source for OIB. (7) Melt thus formed on top of the 410 km boundary will eventually return to the deeper mantle due to entrainment by downwelling material associated with subducting slabs.

However, the original hypothesis proposed by [*Bercovici and Karato*, 2003] contained a number of loosely defined concepts and was based on then poorly known material properties. Furthermore, some of the geophysical and geochemical consequences of the model were not examined in any detail. During the last a few years, there has been much progress in (i) mineral physics, (ii) geodynamic modeling and (iii) geophysical (geochemical) observations on the issues closely related to this TZWF model. The purpose of this paper is to review the current status of this model in view of these new studies. We first review new experimental observations relevant to melt formation and melt density. Secondly, recent models of water circulation and the influence of re-distribution of radioactive elements on convection pattern will be summarized. This is followed by a discussion of geophysical and geochemical constraints on the model. Consequences of transition-zone melting on electrical conductivity and seismological signatures and the influence of transition-zone melting on trace element distribution will also be reviewed. Finally we will discuss future directions to further test and modify the original model.

2. MINERAL PHYSICS BASIS FOR THE TRANSITION-ZONE WATER FILTER

Melting Relations

In the TZWF model, broadly distributed upwelling materials across the 410-km discontinuity partially melts due to the dehydration of wadsleyite. Flux melting occurs by the presence of impurities (such as hydrogen) and the extent of melting is greater when the solubility of impurities in the solid phases is low. An impurity element such as hydrogen (water) has important influence on melting because it is more dissolvable in a liquid phase than in a solid phase. When an impurity phase is dissolved in a material, its free energy is reduced primarily by the increase in the configurational (mixing) entropy, plus some effects through the change in the intrinsic Gibbs free energy (such as the internal energy and the vibrational entropy). Consequently, when an incompatible phase is present, the Gibbs free energy of a liquid phase is reduced by more than that of a solid phase, resulting in a reduction of the melting temperature. However, since the conditions for melting are controlled by the relative Gibbs free energies of melt and solid, the actual melting conditions also depend on the solubility of impurities in the solid phase. The solubility of hydrogen in wadsleyite is larger than that in olivine by roughly 3-10 times at conditions near 410-km (e.g., [*Kohlstedt, et al.*, 1996]). Consequently, the partial melting of upwelling current across the 410-km discontinuity is a key feature of the TZWF model (e.g., [*Bercovici and Karato*, 2003; *Gasparik*, 1993; *Ohtani, et al.*, 2000; *Young, et al.*, 1993]).

Although the basic physics and chemistry of hydrous silicate melts (and with other incompatible elements) is well known, important details regarding the possibility of melting at ~410-km remain poorly constrained. Experimental difficulties in this area include: (i) melts under these conditions are unquenchable and consequently the water content in melts cannot be determined directly from quenched samples, and (ii) small degrees of melting are hard to identify particularly because the dihedral angle of melt and solid minerals under these conditions becomes zero [*Yoshino, et al.*, 2006]. Also, the influence of other incompatible components such as potassium, sodium and/or carbon is critical in estimating the conditions for formation of a dense melt, have not been considered in the previous transition-zone water filter model (e.g., [*Bercovici and Karato*, 2003; *Hirschmann, et al.*, 2005]). Controversy surrounding the calibration of water content [*Bell, et al.*, 2003; *Koga, et al.*, 2003] (see also [*Aubaud, et al.*, 2006; *Karato*, 2006b]) complicates estimates of the amount of water needed for melting from experimental observations.

Considering these complications, we believe that the best approach is to illustrate the range of behavior using a simplified generic phase diagram (Fig. 1). Let us consider melting of mantle material and the presence of water as a simplified pseudo-binary system composed of "silicate" and "water". The "silicate" may contain incompatible components other than water such as K_2O, CO_2 and Na_2O that will affect the melting behavior. For simplicity, the "melting temperature" of water-free peridotites is shown only by one value, T_2 or T_3 for the upper mantle and transition zone materials respectively. This is a good approximation for the melting of impurity-free peridotites in the deep upper mantle for which the solidus and the liquidus are close (e.g., [*Takahashi*, 1986]). However, in cases where the influence of volatile components such as K_2O, CO_2 and Na_2O other than water is important, these temperatures must be interpreted as the solidi corresponding to appropriate systems (in these cases, a phase diagram in at least three-dimensional space is needed to fully characterize the melting behavior).

Fig. 1 illustrates this point. The mantle rocks without water melt at a certain temperature range (T_2 or T_3). When water is added, then water is distributed between the melt and the solid. Water is dissolved into the melt more than in the solid minerals, and hence the melting temperature will be reduced. Now we have two phases (melt and mineral) coexist at a given P and T each of which has a certain amount of water that is controlled by the partitioning coefficient. Each curve describing the composition and T (P) for each coexisting phase will define the solidus and the liquidus. In Fig. 1, the curve T_2-Q is the solidus, and the curve T_2-X_1 is the liquidus for the upper mantle phase (for the transition zone minerals

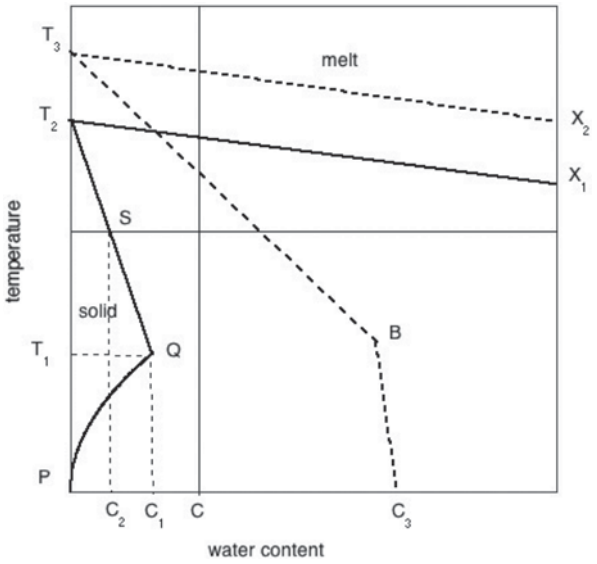

Fig. 1. Schematic phase diagram for a theoretical binary system of silicate + water at ~410 km. Thicker dashed and solid lines represent the solidus for transition zone and upper mantle minerals, respectively. The curve $P-Q$ (thin dashed line) represents the solubility of water in upper mantle minerals as a function of temperature. Above a certain temperature (T_1), a water-rich fluid/melt forms and the amount of hydrogen in solid minerals coexisting with the hydrous melt decreases with temperature (trend Q–S –T_2). Given the curves $T_2 - X_1$ (liquidus) and Q–S –T_2 (solidus), one can infer the critical water content for melting and the water content in the melt (for details see text).

$T_3 - B$ is the solidus, and $T_3 - X_2$ is the liquidus). The low temperature portions of the phase diagram can be analyzed using the experimental data on the solubility of water in the solid minerals. At low temperatures, a fluid phase that would coexist with the minerals will be free water. Solid minerals have a certain degree of solubility of water. Therefore the phase diagram at low temperature is characterized by a curve P-Q that is essentially the solubility of water in the upper mantle minerals (the solubility of water in the transition zone minerals is much higher and is shown by a curve $C_3 - B$). When water starts to dissolve silicate components, then the fugacity of water in the system will be lowered. As a consequence, the amount of water dissolved in the solid minerals will be reduced. Eventually, the fluid phase becomes indistinguishable from silicate melt, and the solubility curve should become the solidus curve. The inflection point Q defines the temperature at which the solubility of silicates in water becomes large.

Let us first discuss the curve T_2-Q, the solidus of the upper mantle rocks, which defines the conditions for melting. T_2 is the melting temperature (or the solidus) without water. The

melting temperature (the solidus) of the upper mantle rock without any volatiles is well constrained. It is ~2400 K at 410-km (e.g., [*Inoue*, 1994; *Ohtani, et al.*, 1995; *Takahashi*, 1986]).

The point *Q* is determined by the solubility of water in mantle minerals and the solubility of silicates in water. The solubility of water (hydrogen) in olivine is well-constrained ([*Kohlstedt, et al.*, 1996; *Zhao, et al.*, 2004]), and some less detailed data are available for other minerals such as garnet. However, the solubility of silicates in water is not well constrained. Because of the lack of well-defined eutectic melting behavior due to the total miscibility between silicate melts and water at high *P*, the point *Q* is not well defined. However, [*Stalder, et al.*, 2001] showed a change in properties of hydrous melt at T~1500 K (at P~14 GPa). Therefore we use this temperature as a rough estimate for the inflection point *Q*. The experimental studies by [*Inoue*, 1994; *Inoue and Sawamoto*, 1992] show the results that are consistent with this choice of inflection point. The water solubility in olivine at the point *Q* (T~1500 K and P~14 GPa) is ~0.1 wt%. The total water solubility in upper mantle rocks at this condition depends also on the water solubility in other minerals. Currently there is a large discrepancy on the water solubility in garnets (e.g., [*Lu and Keppler*, 1997; *Withers, et al.*, 1998]). Also the water solubility in pyroxenes is not well constrained under deep upper mantle conditions (e.g., [*Mierdel and Keppler*, 2004; *Rauch and Keppler*, 2002]) (for a review of the experimental data see also [*Bolfan-Casanova*, 2005]). In this paper, we tentatively use the solubility value in olivine C_W~ 0.1 wt% (and T_1~1500 K) to define the conditions at $Q(C_W - T_1)$. The estimated water content at *Q* has an uncertainty of a factor of ~2 caused by the uncertainties in the water solubility in garnet and pyroxenes and in the FT-IR calibration.

The solidus, $Q - S - T_2$, can be estimated by the interpolation between two fixed points, T_2 and $Q(C_W,T_1)$. The solidus line has a curvature such that it should be concave downward in this plot, but considering the large uncertainties, we use a straight line. If T_2 for volatile free upper mantle (~2400 K) is used, and if the typical mantle temperature of ~1800-2000 K at 410-km is used, then the critical water content is estimated to be ~0.05 wt%. The critical value of water content for partial melting estimated here is much less than the value estimated by [*Hirschmann, et al.*, 2005] (~0.4 wt%) with which one would conclude that melting is highly unlikely in most of the current Earth's mantle at ~410-km. This is due to the fact that [*Hirschmann, et al.*, 2005] essentially identified the solubility limit of water in upper mantle minerals at the eutectic point, *Q*, as the solidus. The water content in olivine at the solidus at a higher temperature (S) will be significantly lower than the water content at *Q*. The solubility of water (hydrogen) in minerals and the water content at the solidus (which defines the minimum water content for melting) are different and should not be confused.

So far, we have only considered the influence of water on partial melting. It is well known that Earth contains other incompatible elements such as carbon, potassium and sodium that partition into the melt (e.g., [*McDonough and Sun*, 1995]). Consequently, these elements should play a similar role in the melting as hydrogen. Experimental studies on melting of upper mantle peridotites have shown that these impurities reduce the melting temperature of dry peridotite (see Table 1). Consequently, for the water-free but otherwise impurity-present mantle, the solidus temperature, T_2, will be ~1800-2000 K at ~410 km as opposed to ~2400 K for volatile-free peridotite. Note that this temperature is close to the estimated temperature at 410-km (~1800-2000 K; e.g., [*Ito and Katsura*, 1989]). In fact, [*Wang and Takahashi*, 2000] suggested a wide-spread (small degree of) partial melting in the transition zone due to the influence of K_2O. The influence of incompatible elements on melting is essentially through their effects on the configurational (mixing) entropy, and hence the conditions for melting at a given temperature and pressure is determined by the net molar abundance of incompatible elements. Consequently, the minimum amount of water to cause partial melting at 410-km is reduced when other incompatible elements are present. We conclude that the minimum amount of water needed for melting is ~0.05 wt% or less for a realistic mantle where other impurities are also present. When the estimated critical value of water content for melting is compared with the recent estimate of water contents in the transition zone (~0.1-0.2 wt% in the Pacific; [*Huang, et al.*, 2005; 2006], up to ~1 wt% in the western Pacific or the Philippine sea region; [*Suetsugu, et al.*, 2006]), we conclude that partial melting at or near 410-km is likely in a broad region of the current Earth's mantle.

The Melt Density

One of the direct consequences of this type of melting (*flux melting*) is that the melt produced should have a large concentration of incompatible elements, and the amount of incompatible elements in the melt increases with a decrease in temperature. To be more specific, "pure" peridotites (peridotites with little or no volatile, incompatible elements)

[1] [*Hirschmann et al.,* 2005] began their discussion by distinguishing the solidus and the solubility limit, but in their final estimate of the minimum water content for melting, they used the solubility limit.

Table 1. Amount of reduction in solidus of peridotite by volatiles at ~14 GPa

CO_2	~400 K	eutectic*	[*Dasgupta and Hirschmann*, 2006]
K_2O	~600 K	eutectic*	[*Wang and Takahashi*, 2000]
Na_2O	~150 K	for 0.3 wt%	[*Hirschmann, et al.*, 1998]
H_2O	~600 K	for 2 wt%	[*Litasov and Ohtani*, 2002]

*: For eutectic melting, the solidus reduction is independent of the concentration of impurities. However, the notion of "eutectic" behavior is not well documented in these studies. A small amount of solubilities of these elements in the mineral will change the melting behavior to solid-solution type as shown in **Fig. 1.**

will melt at ~2400 K at ~410-km depth (e.g., [*Inoue*, 1994; *Inoue and Sawamoto*, 1992; *Ohtani, et al.*, 1995; *Takahashi*, 1986]). A plausible temperature at 410-km discontinuity is ~1800-1900 K for typical regions, and ~2000-2100 K for hot regions (i.e., plumes or the Archean mantle). Therefore one needs to have a large enough concentration of impurities to reduce the solidus by ~300-500 K.

The concentration of incompatible elements in the melt depends strongly on the degree of melting temperature reduction needed to cause melting. A simple thermodynamic analysis shows that a decrease in melting point by incompatible elements is due mainly by their effect of increasing the configurational entropy of a melt, thus $\delta S_{config} = \Delta S_m \frac{\delta T}{T_m}$ where δS_{config} is the change in configurational entropy, ΔS_m is the entropy change upon melting, T_m is the melting temperature, and δT is the reduction of melting temperature. Because δS_{config} is a function of concentration of incompatible elements, equation $\delta S_{config} = \Delta S_m \frac{\delta T}{T_m}$ gives a relation between the concentration of incompatible elements and melting temperature reduction. At deep mantle melting, $\Delta V_m \sim 0$ and $\Delta S_m \approx R log 2 = 0.69$ R and hence $\delta S_{config} \sim 0.15$ R ~ for T_m=2400 K and δT =500 K. This can be translated into the (molar) concentration of impurities, x, through $S_{config} = -R\left[x log\, x + (1-x) log(1-x)\right]$ to $x \sim 0.35$. Experimental studies show that ~10-15 wt% of water is dissolved in the melt at P~14GPa to reduce the melting temperature by ~500 K ([*Litasov and Ohtani*, 2002]). If all hydrogen is in the form of H_2O, this will correspond to x=0.15-0.22, whereas if all hydrogen in the form of OH, x=0.30-0.45. We conclude that the experimental observation by [*Litasov and Ohtani*, 2002] agrees with a simple model and a molar fraction of impurity on the order of ~0.2-0.4 is needed to cause melting at 410-km at a temperature of ~1900 K.

Incompatible elements such as hydrogen enhance melting, but the addition of incompatible elements also influences melt density. Being the lightest element, the addition of hydrogen significantly reduces the density of a melt. [*Matsukage, et al.*, 2005] determined the influence of water on the density of peridotite melt. The density of water in the peridotite melt at P~14 GPa and T~1900 K is ~2.3 $\times$ 10^3 kg/m^3 (molar volume ~8x10^{-6} m^3/mol), and comparable to effects of H2O on the density MORB melt [*Sakamaki et al.,* 2006].

Given the molecular weights and the partial molar volumes of incompatible components, one can estimate the density of melt and examine the critical concentrations of incompatible components needed to produce a melt denser than the surrounding solid mantle at 410-km. *Matsukage et al.* [2005] calculated the critical water contents for a dense peridotite melt at ~410-km conditions (P=14 GPa, T~1900 K) and obtained a value of ~5 (+7, -2) wt% ([*Sakamaki, et al.*, 2006] obtained a similar result for MORB). Although uncertainties are very large, these values are less than the estimated water content in the melt under similar conditions (~10-15 wt%) and we conclude that the conditions for a dense melt are limited if only water is considered.

Water is the lightest impurity component, but in the mantle there are expected to be other impurities with higher density components that have higher densities (Table 2). Based on the above analysis, we now assume that a total amount of impurity is ~0.2-0.4 (molar fraction) through a combi-

Table 2. The abundance and properties of typical "impurity" components

	molecular weight	abundance[1]	density[2]	partial molar volume
H_2O	18	50-1000 (wt ppm)	2.3 ($\times$ 10^3 kg/m^3)	8 ($\times$ 10^{-6} m^3/mol)
CO_2	44	1200	2.9	15
Na_2O	62	6200	3.2	19
K_2O	94	300	3.4	28

[1]: water: see papers in this volume, carbon dioxide: [*Dasgupta and Hirschmann*, 2006], Na_2O: [*McDonough and Sun*, 1995], K_2O: [*McDonough and Sun*, 1995].

[2]: The densities and partial molar volumes of these species in silicate melt at P=14 GPa and T=1900 K. The data for water is from [*Matsukage, et al.*, 2005], the density of CO_2 is estimated from the equation of state (e.g., [*Frost and Wood*, 1997]), and those for Na_2O and K_2O are calculated from low P data using the Birch-Murnaghan equation of state for K'=6 with the initial density and K_o summarized by [*Lange and Carmichael*, 1990]. The uncertainty in the density (partial molar volume) estimate is ~±20%.

nation of impurities (K_2O, Na_2O and CO_2). The critical ratio of water to other impurities is $\frac{C_W}{C_X}$ (C_W: molar content of water, C_X: molar content of another volatile impurity such as K_2O). For example, K_2O is heavy and makes a melt denser when K_2O is added (Fig. 2). For a total impurity content of 0.3, the critical value of $\frac{C_W}{C_X}$ is ~0.4 (when C_X is the molar content of K_2O). When the fraction of water exceeds this critical value, then the melt will be light and the water filter leaks. Regions with a very high water content (geochemically "enriched" regions) will undergo melting at ~410-km but the melt will be light and filtering will not occur. These materials will form OIB with enriched geochemical signature upon melting near the surface. Whereas when the fraction of water content is less than this value but the total volatile content is large enough for melting to occur, then the melt is dense and the water filter will work, and a depleted materials after filtering will become the source materials for MORB. Finally, when the total amount of volatiles is too low, then melting does not occur and the water filter will not work. These materials will rise to form MORB or relatively depleted OIB. An important conclusion is that the water filter will work only when the water content is in an intermediate range. We note that the above estimates of critical conditions for a dense melt have very large uncertainties for two reasons. First, the estimate of the partial molar volumes of volatile components contains large uncertainties (see Table 2). Second, the estimate of the critical molar concentration of volatile from experimental studies has large uncertainties. Consequently, the above values must be considered as rough estimate only.

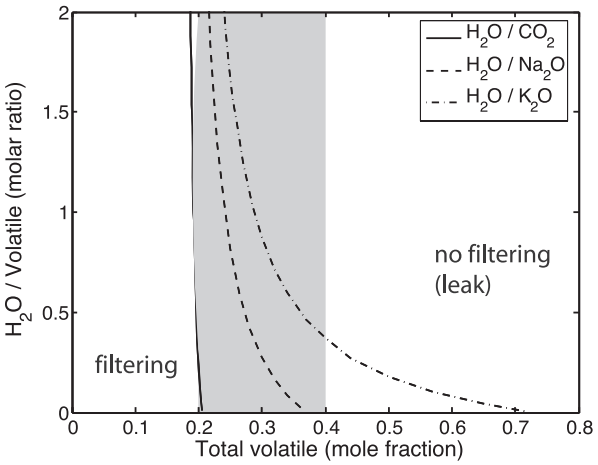

Fig. 2. Critical conditions (in terms of volatile composition) for which water filter works. When the density of melt generated at ~410-km is denser than that of the surrounding upper mantle minerals (but lighter than the transition-zone minerals), then water filter will work. The total volatile content needed for melting at ~410-km is difficult to calculate mainly because of (i) a large uncertainty in the partial molar volume of water (this diagram assumes 8 cm^3/mol) and (ii) a large uncertainty in the experimental determination of volatile content but is estimated to be 0.2–0.4. For a given total volatile content, there is a maximum water content (relative to the concentration of other volatiles) at which the melt is dense and the water filter works. In regions where the water content is very high, the melt will be light and the filter will leak.

The new experimental data on melting relationship and the density of hydrous melt indicate that the conditions under which water-filter mechanism operates depend critically on the concentration of incompatible components (as well as the mantle temperature). The previous studies on melting and melt density have been focused on the influence of water only. When only the influence of water is considered, although partial melting likely occurs in most cases (melting occurs if more than ~0.05wt% of water is present), the melt thus produced will probably be lighter than the surrounding solid minerals because the reduction of melting temperature can be achieved only by dissolving a large amount of water in the melt.

However, considering other incompatible impurities such as CO_2, K_2O or Na_2O, flux melting and the formation of denser melt is possible. We conclude that partial melting in the deep mantle at ~410-km is highly likely, and a melt of sufficient density to remain neutrally buoyant at ~410 km will include CO_2, K_2O or Na_2O in addition to H_2O. In a typical oceanic upper mantle, current estimates of water content in the transition zone are small (~0.1 wt%), and the major impurity components in the melt are K_2O or Na_2O. However, in regions of the transition zone where subduction occurs, higher water contents of ~1 wt% are inferred (e.g., [*Suetsugu, et al.*, 2006]). In these cases, melt would contain a large amount of water and be less dense than the surrounding mantle and hence rise and result in volcanism. Some volcanism away from the trench could be due to melting of subducted material with higher water contents. ([*Iwamori*, 1992; *Miyashiro*, 1986]). Some OIBs may be formed by the upwelling of relatively water-rich materials that do not undergo filtering because of the low density of melt.

3. MODELS OF MATERIAL CIRCULATION

Simple Mass-Balance Box Model (Appendix I)

In this section, we review theoretical modeling of dense partial melt at ~410-km and discuss plausible processes by which volatile components such as water are entrained and circulated through the transition zone. In the original TZWF study, [*Bercovici and Karato*, 2003] proposed a simple mass balance or box-model calculation to illustrate the basic predictions of their hypothesis. We briefly review the primary

ingredients of this model in order to establish the setting for further unanswered geodynamical questions. In particular, we discuss in some detail the assumptions made in constructing this box model, and where recent developments shed new light on these assumptions.

The putative heavy melt-rich layer at the 410-km boundary that is predicted by the TZWF model is assumed to reach a steady thickness once the melt production from the mantle upwelling is balanced by melt entrainment from slab-induced downwelling (see sections below). Since the melt is heavy it will accumulate and the solid matrix will decompact or dilate to accommodate the pooling of heavy melt. However, the matrix will not necessarily completely decompact if the melt is drawn away by slab-associated entrainment is fast enough; i.e., the pooling of heavy melt drives decompaction but the melt could be extracted efficiently enough that the matrix never completely decompacts. Two-phase compaction theory [*Bercovici and Ricard*, 2003; *Bercovici, et al*., 2001; *McKenzie*, 1984] can be used to infer basic scaling relationships between the peak porosity Φ in the melt-rich layer, the melt-rich layer thickness, H , and the slab-induced entrainment rate U. These relations are shown in Fig. 3 for an input melt fraction of f = 1%. First, we can see that increasing slab entrainment rate U causes both Φ and H to decrease because as the entrainment is more efficient it both keeps the melt-rich layer thinner and suppresses decompaction of the matrix. H scales with $H^* \equiv \sqrt{\frac{\mu_m W}{|\Delta\rho| g}}$ (μ_m: solid viscosity, W: ambient mantle upwelling velocity (~10^{-11} m/s ([*Bercovici and Karato*, 2003]), $|\Delta\rho|$: density difference between melt and solid). The thickness of the melt-rich layer is sensitive to the solid viscosity and the density contrast. For typical values of $|\Delta\rho|$~10 kg/m^3 and μ_m ~10^{18} Pa s, H~1 km (however both parameters can vary by orders of magnitude that leads to a broad range of H: for example, if melt completely wets grain-boundaries under deep mantle conditions as suggested by [*Yoshino, et al*., 2006], then μ_m will be considerably lower than the above value). Because this melt-rich layer is probably thin (for typical values of parameters), detection of this layer by seismology will require a high-resolution technique that is sensitive to the impedance contrast.

In the essential TZWF hypothesis, water is assumed to be trapped within the transition-zone because of dehydration melting of ambient upwelling at 410 km, and by exolution of water from slabs at 660km [*Bercovici and Karato*, 2003], [*Richard, et al*., 2006a]. Without the production of liquid phases above and below the transition-zone, water would tend to be largely removed and homogenized throughout the mantle [*Bercovici and Karato*, 2003; *Richard, et al*.,

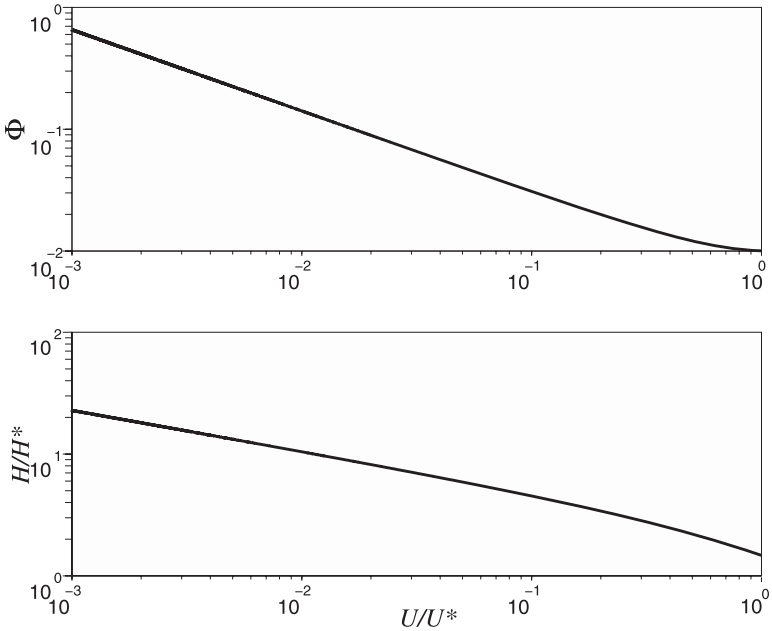

Fig. 3. Steady state scaling relationships for peak porosity Φ and melt layer thickness H versus slab-induced entrainment rate U for the putative heavy melt layerp at 410km (see Appendix I). The melt layer thickness scale is $H^* = \sqrt{\mu_m W/(|\Delta\rho|g)}$, and the entrainment rate scale is U ∗ = scale is $\sqrt{W|\Delta\rho|g/\mu_m}$, where W is the ambient mantle upwelling velocity, μm is the solid matrix viscosity, Δρ < 0 is the solid-melt density difference, and g is gravity. Input melt fraction (i.e., of the upwelling mantle) is fixed at f = 1%. See text for discussion and Appendix I for details.

2002]. Of course, the complete entrapment of water in the transition-zone is an end-member case since some leakage is bound to occur (since the upper and lower mantle phases above and below the transition-zone can transport some water, albeit at small concentrations.) With the assumption that recycling of water is primarily closed in the transition-zone (with any leakage largely compensated by input from slabs transporting water from the surface), we posed a simple theoretical mass-balance model with which to understand, for example, the average thickness of the melt layer.

The model system is driven by a background circulation through the transition-zone consisting of downwelling slabs and the resultant passive ambient upwelling. The slab mass flux is in fact the primary driver of the entire system. We assume that the majority of the upwelling mantle rises passively in response to downward slab injection, and that plumes play only a minor role in the upward mass flux. This simple picture of mantle circulation is in keeping with standard models of convection where the heat source is primarily from radiogenic heating and secular cooling, both of which lead to a "top-cooled", downwelling dominated system. The net slab flux is calculated assuming a downwelling rate of order 10 cm/yr (or less), an average slab thickness of approximately 100 km, and a global slab length approximately equal to the circumference of the Earth (since most of the slab flux occurs in a nearly great circle around the Pacific ring of fire). A mass-flux balance calculation thus leads to a globally averaged passive mantle upwelling of around 1 mm/yr.

Continuous influx of melt into the 410km melt layer would eventually lead to an ever thickening melt layer that could possibly reach the density cross-over point and start to ascend; it if ascends through percolation it would essentially recontaminate the upper mantle, undoing the filter mechanism. If it ascends through diapiric instabilities (depending on how compacted and impermeable the solid is above the melt layer) then the melt and solid might remain isolated, allowing for the arrival of depleted MORB-source mantle; however, this would also suggest the arrival of very highly enriched wet melts in anomalous midplate or non-MORB magmatism.

A more likely scenario is that the heavy melt layer interacts with downwelling mantle and is entrained back into the lower mantle. Indeed, the melt layer can reach a steady state thickness and composition if its material is removed by slab induced entrainment at the same rate it is injected by upwelling ambient mantle.

In the original TZWF model, entrainment is assumed to occur solely by freezing of melt onto slabs (or within the slabs' cold thermal halo). Cooling and freezing of the melt near slabs is facilitated by "window-pane" convection (driven by cooling of fluid from the side) and leads to a thick silicate solidification entrainment zone [*Bercovici and Karato*, 2003]. However, the solidified material cannot remove water in sufficient quantities. That is, the silicates crystallize at the wadsleyite saturation value of a few percent (since, at cold near-slab temperatures, the melt solidifies to wadsleyite) which is much less than the melt's water concentration of perhaps tens of percent. Thus solidification of melt leaves large quantities of water, which likely just dissolve in the nearby melt. So water must be removed by additional means. Entrapment of melt and/or exsolved water by inclusions in the solidifying material is unlikely since the solid fraction is probably not large enough and the melt/water pathways not closed (again the dihedral angles are probably nearly zero). In our original model [*Bercovici and Karato*, 2003], the other likely water-removal mechanism was assumed to be chemical diffusion of water. The accumulation of water in the melt would put the melt well beyond chemical equilibrium with the slab and thus diffusion of water into the slab could occur at a sufficient rate to remove the water. In fact, this was one of the main elements of the self-limiting feature of the model that allowed steady state. If water removal was inefficient, then the melt layer would thicken and water would accumulate near the slab; however, the melt layer thickness also represents the slab-melt contact area and the thicker the layer the more water could diffuse into the slab. Thus eventually a thickness could be reached that would allow for the all the water as well as silicates to be removed at the same rate that they were injected by mantle upwelling.

Box-Model Predictions

With the assumptions of slab entrainment, one could calculate a melt layer thickness and overall distribution of water in the melt-layer–transition-zone system. However, such model calculations only indicate the effective thickness of a pure melt layer averaged over the entire globe: they do not account for lateral variations in melt layer thickness, nor do they estimate thickness of a partial melt layer which would conceivably be thicker but have different mechanical properties. Nonetheless, simple box-model results predicted an average effective melt layer thickness on the order of a few tens of kilometers. More recent analyses (discussed below) considers more realistic conditions to estimate melt layer structure.

However, sufficient filtering of the upwelling mantle also required water diffusivity at least an order or magnitude higher than that for olivine (i.e., higher than $10^{-8} m^2/s$). Otherwise, a diffusivity that is too low can only be compensated by thick melt layer, which would take up almost all the water of the system, leaving the transition-zone too dry to produce sufficient melt fractions to allow the filter to work.

In our original work, we argued that water diffusivity in wadsleyite was likely to be as much as 3 orders of magnitude

faster than in olivine; no experimental evidence for this was known, although it was thought that the much higher diffusivity of other elements and the higher electrical conductivity in wadsleyite indicated the likelihood of a higher water (i.e., hydrogen) diffusivity. In this case, diffusive entrainment of water by slabs was a plausible mechanism. Yet, recent studies of water diffusivity in transition-zone minerals suggest that it is probably no faster than in olivine [*Hae, et al*., 2005] which casts doubt on the slab/water-diffusion entrainment assumption. Moreover, preliminary work by our group [*Leahy and Bercovici*, 2006] indicates that the slab entrainment model is a serious oversimplification and that entrainment is a continuous process driven by chemical reaction with dry downwelling mantle and not only by freezing at the so-called interface between the melt and the slab. This new development is discussed below.

Entrainment by Reaction With Downwelling Mantle: Viscous Entrainment Zone

As described above, the original TZWF model stipulated that the melt layer was essentially divided into two regions: a melt production area, where wet upwelling material melts as it passes the 410km boundary, and a slab-entrainment area, where the melted material refreezes as it comes into contact with cold slabs, leading to its entrainment into the deeper mantle. However, this is an oversimplification in many ways, most notably in that it assumes the mantle makes an abrupt transition from upwelling (where melt is produced) to the downwelling slab region (where melt is removed). Being highly viscous, the mantle obviously cannot support such abrupt transitions in flow directions, so clearly there is a continuous change in the upwelling velocity, from its peak value (roughly at some point furthest from slabs, or equidistant from encircling slabs) through zero, across a relatively broad downwelling region being viscously dragged down by slabs, then to the maximum downwelling velocity at the cold slab itself. The region viscously entrained by slabs is roughly at ambient mantle temperatures, as typical for infinite Prandtl number systems where thermal diffusivity is much less than momentum diffusivity. The melt produced in the upwelling region will tend to spread under its own weight into this *viscous entrainment zone* (VEZ) and begin to react with the downwelling ambient mantle in a somewhat complicated mechanism we have proposed [*Leahy and Bercovici*, 2006] and describe below (Plate 1).

Reaction Between Melt and Viscous-Entrainment Zone

In the upwelling melt-production region, the heavy melt and the remaining buoyant solid are at, or nearly at, chemical equilibrium with respect to water since partial melting is assumed to occur at equilibrium. As the melt spreads into the ambient downwelling, or viscous entrainment zone, it comes into contact with downgoing solid upper mantle that might at best be hydrated enough to still be near equilibrium with the melt (i.e., if the solid has remained unprocessed since passing through the 410km filter), or more likely is relatively dry (assuming further processing by continued melting during upwelling, or further melting at ridges or beneath the lithosphere) and thus well away from equilibrium with the melt. However, the downward traversal of this solid upper mantle material across an ostensibly heavier melt is a nontrivial process. In fact, a key step in the process is that melt is pushed or advected by the downwelling into the wadsleyite stability field, where (because of the higher wet-melting temperature of wadsleyite) the melt freezes (Fig. 4). Although silicates in the melt solidify as water-saturated wadsleyite, the melt's water concentration is much larger than the saturation limit for ambient wadsleyite (of order 1%) and so water is exsolved in the freezing process and, being buoyant, ascends to be reabsorbed by the overlying melt. The melts water concentration thus rises and given the melt's low viscosity, the water concentration of melt also homogenizes relatively quickly. This causes the hydrous melt to be out of equilibrium with the overlying downwelling olivine (even if the olivine had remained unprocessed); the melt thus reacts with the olivine (i.e., hydrates it locally beyond its saturation value) causing the olivine to melt, and likewise acting to dilute the melt with additional silicate (thus reducing its water concentration). However, in this downwelling region the entire process (i.e., the melt layer being pushed and frozen into the transition-zone, the melt becoming subsequently "super-hydrated", and thus olivine reacting and melting into the melt layer) is ongoing and allows the traversal of downgoing material across the melt zone.

In the original simple slab entrainment model, the accumulation of water near the slab purportedly lead to an enhanced diffusion flux of water into the slab. But within the viscous entrainment zone, the accumulation of water is readily damped out by reaction with olivine downwelling from above. A large diffusive flux is probably never necessary to effect melt and water entrainment with this viscous-entrainment mechanism (other than perhaps to hydrate the overlying olivine, but this is also driven by reaction rates and occurs along reaction fronts where local equilibrium is maintained, thus hydrogen diffusion across a thin or infinitesimal reaction front is nearly instantaneous).

Quite significantly, this "viscous-entrainment-zone" process provides an extremely important means for draining the melt layer back into the lower mantle. As with simple slab entrainment, water in the melt can only be drawn back into the transition-zone at wadsleyite saturation concen-

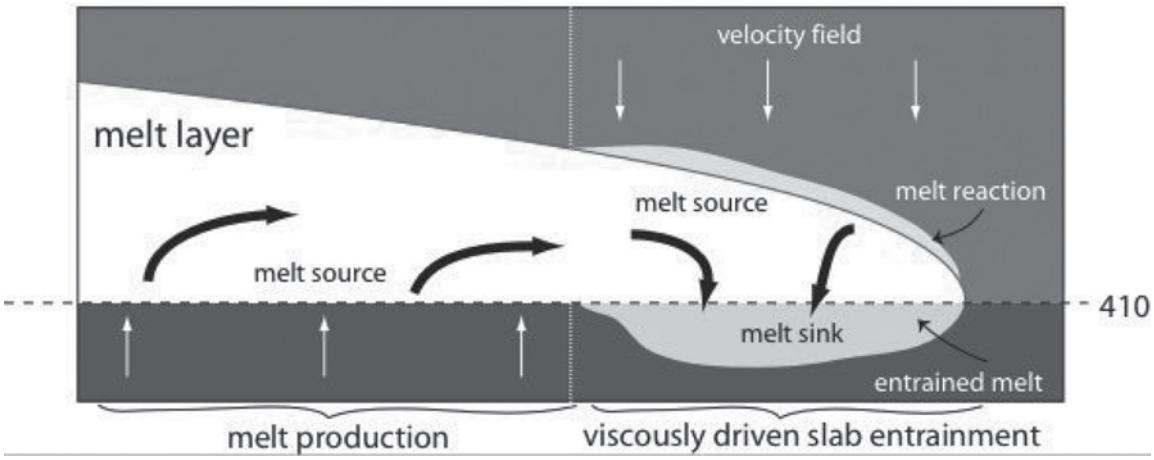

Fig. 4. Model melt layer structure as a spreading gravity current with sources of melt in upwelling regions, and net sink of mass in downwelling regions, where entrainment is accompanied by a melting reaction at the top of the melt layer

trations. However, the melt is entrained over a potentially much broader region (i.e., as much as the entire viscous entrainment zone) rather than just along the melt-slab contact. Since water is essentially only being injected from the transition-zone at roughly 0.1 wt% through the broad upwelling, and taken back down at saturation value of roughly 1 wt%, then water can be drained with a downwelling mass flux roughly 1/10th that of the upwelling mass flux. Indeed, simple calculations indicate this mechanism is extremely efficient at draining the melt layer and could by itself keep the melt zone extremely thin. However, as discussed below [*Leahy and Bercovici*, 2006] the entrainment also affects the background flow which then likely inhibits the entrainment process itself (Fig. 5).

An important implication of the aforementioned "viscous-zone" entrainment mechanism is that material from the melt layer that gets solidified and recycled into the transition-zone has a large, near saturation water content and is thus relatively buoyant [see *Jacobsen*, 2006 for a review of related equations of state]. [*Leahy and Bercovici*, 2006] find that though this hydrated material is embedded in the downwelling, its buoyancy is sufficient to impede the slab-driven flow field (Plate 2). The reduction in downwelling mass flux and melt drainage allows the melt layer to thicken and spread further across the viscous entrainment zone before being drawn away. Earth-like parameter regimes are characterized by competition between buoyant spreading of hydrated wadsleyite and slab-driven downward entrainment. Buoyant spreading of hydrated material tends to spread laterally in the transition zone and drives small scale chemical circulation within the transition-zone, which has a further—albeit more complicated—feedback on melt production and melt drainage.

The drainage of water into the transition zone over a relatively broad viscous entrainment region, and the subsequently induced secondary circulation via chemically driven convection, provides a mechanism for recirculating, mixing and distributing water in the transition zone. In the original TZWF model with simple slab entrainment, water would be returned to the transition-zone in a nearly closed-system cycle. However, the model did not specify how water would be mixed and distributed across broad areas of the transition zone in order to continue to hydrate the broad upwellings rising out of the lower mantle. Drainage of water into the transition-zone through the broad viscous entrainment zones begins to address this important question. Moreover, secondary circulation established by chemical convection would also facilitate mixing in the transition-zone.

Hydration of the Transition-Zone by "Stagnant Slabs"

The water entrainment processes discussed above provides some possible mechanisms for water recycling and distribution in the transition zone. Another important recirculating mechanism concerns slab-induced entrainment and the prevalent horizontal deflection of slabs in the transition zone [*Richard, et al.*, 2006]. The horizontal deflection of many slabs in the transition zone is well documented from seismic tomography [*Fukao, et al.*, 1992; *Fukao, et al.*, 2001; *Zhao*, 2004]. Hydrated material from the oceanic crust and lithosphere, as well as from the putative 410km melt layer that is entrained by slabs either within the slabs cold thermal halo as originally proposed by [*Bercovici and Karato*, 2003], or through the viscous entrainment zone as proposed by [*Leahy and Bercovici*, 2006] and discussed above, would be horizontally deflected

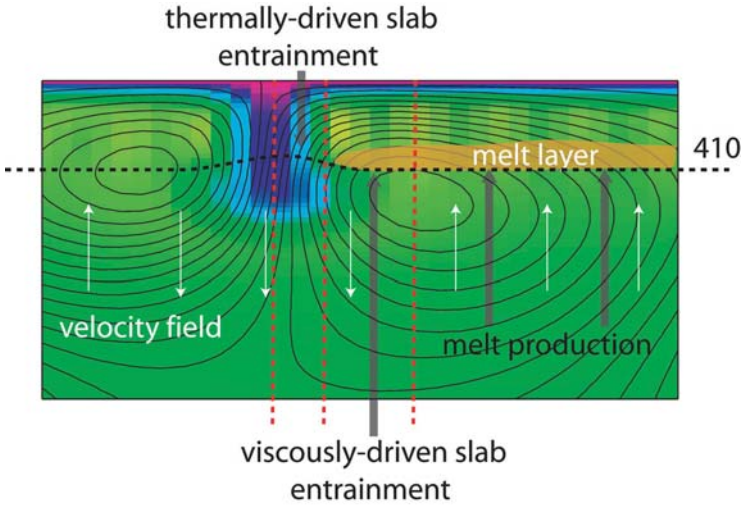

Plate 1. The flow field from a convection simulation demonstrates possible water-filter regimes: melt production, where hydrated wadsleyite is advected above the 410 km discontinuity and melting occurs, thermally-driven slab entrainment ([*Bercovici and Karato*, 2003]), where melt is entrained primarily due to diffusion of water into cold slabs, and viscously-driven slab entrainment, where melt is entrained into downgoing wadsleyite at ambient mantle temperatures (after [*Leahy and Bercovici*, 2006]).

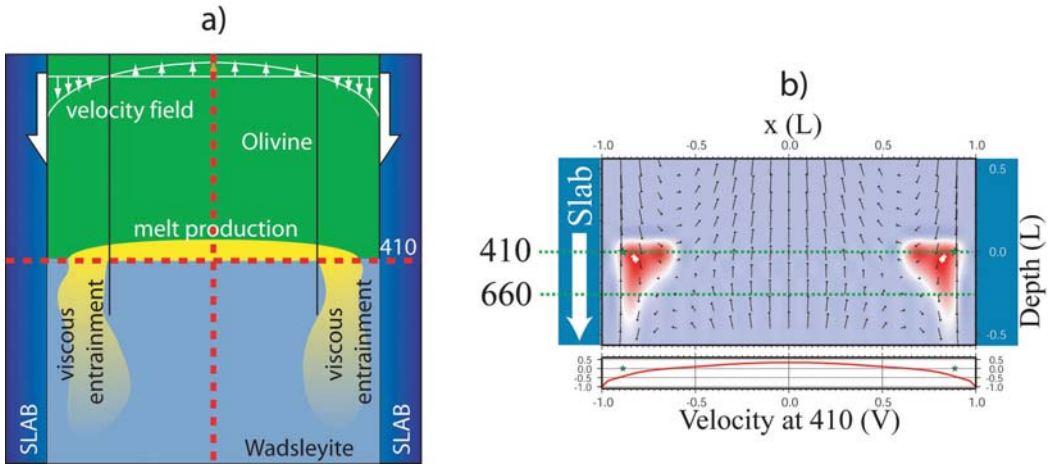

Plate 2. Buoyancy effect of entrained melt on mantle flow. a) A simple slab-driven velocity model is perturbed due to buoyancy anomalies of entrained melt at the 410. b) Calculations of the new flow field (arrows) and steady-state water distribution for the model. Red areas are enriched in water relative to the background (blue). Entrained melt permits the melt layer to spread further through adjustments to the velocity field, and may contribute to the rehydration of the transition zone.

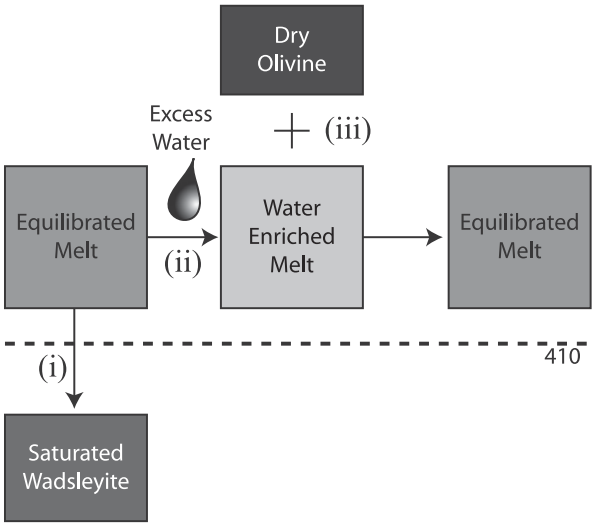

Fig. 5. Flow chart showing the chain of events when a small amount of the melt is dragged below the 410-km discontinuity. (i) The melt is in equilibrium with wet wadsleyite, which crystallizes out of the melt and continues to sink. (ii) The water excess due to crystallization stays in the layer and enriches the melt, which is now out of equilibrium with the overlying olivine solid. (iii) The enriched melt reacts with the olivine, causing melting to return the system to equilibrium. This provides a mechanism for the melt to spread further into the viscous entrainment region.

with the slab, and the upward-facing side of the slab would potentially lose water by diffusive and, if conditions are right, convective transport (Fig. 6).

Diffusive transport of water from the "floating slab" is complicated by the temperature contrast between the cold slab and the overlying "ambient" transition-zone because water solubility is temperature dependent. Even if a system has initially uniform chemical concentration, a contrast in solubility would establish a gradient in chemical potential causing water to diffuse from the low solubility to the higher solubility region until equilibrium is established. Experimental studies [*Demouchy, et al.*, 2005; *Kawamoto et al.,* 1996; *Ohtani, et al.*, 2000; *Zhao et al.,* 2004] indicate that the solubility of water in olivine, wadsleyite, and ringwoodite increase slightly with temperature but only up to temperatures (~1200C) where the system solidus is reached and a melt/fluid forms (see Appendix II). Upon further increase of temperature, as the volume fraction of melt/fluid increases, the amount of water in the coexisting minerals decreases. In the presence of fluid, the storage capacity of water in the minerals decreases rapidly. For example in wadsleyite, the solubility decreases from ~2.5 wt% H_2O at 1400 C to ~1.5 wt% at 1500 C [*Demouchy et al.,* 2005].

Theoretical "double diffusion" studies of coupled diffusive transport of heat into and water out of a floating slab [*Richard, et al.*, 2006b] yield intriguing results. If solubility increases with temperature, thermal gradients enhance chemical transport since the warm mantle overlying the floating slab has higher solubility than does the colder slab, and thus essentially acts to soak up the available water. Alternatively, if solubility decreases with increasing temperature then one nominally expects chemical transport to be inhibited since the warm mantle overlying the slab would have lower solubility than the cold slab. However,

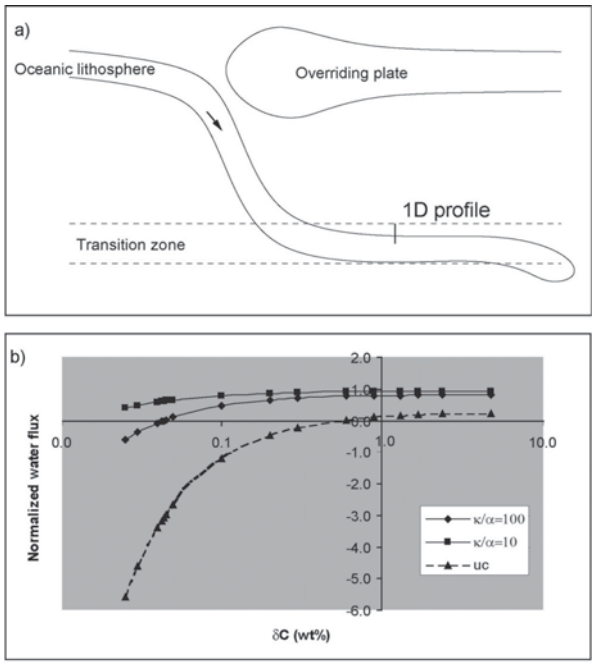

Fig. 6. a) The dehydration of a stagnant slab in the mantle transition zone. The essence of the model hypothesis: The diffusion of water out of the slab and the diffusion of heat into the slab occur simultaneously and are coupled by the temperature dependence of the water solubility. b) Effect of the initial slab water concentration on the outgoing water flux. Normalized water fluxes (NWF: total water flux over pure chemical water flux ratio) as function of the initial water concentration step between slab and mantle (δC (wt%)) for two water diffusivities ($\alpha=10^{-8},10^{-7}$ m^2/s) compared to the NWF if the heat and water diffusion processes were uncoupled (UC, dashed line). The NWF is almost constant and close to one for high slab concentration ($\delta C>0.5$wt%) and decreases rapidly for lower values. This plot demonstrates that the coupling strongly mitigates the decrease of water flux induced by the high solubility of the cold slab (E=-100 kJ/mol is the intrinsic chemical potential of the water in wadsleyite). The thermal diffusivity is set to be $\kappa=10^{-6}$ m^2/s and the mantle water concentration is fixed to 0.1 wt%.

several nonlinear interactions may act to mitigate this effect. First, as the uppermost region of the recumbent, floating and hydrated slab warms, its solubility drops causing it to approach saturation and to be even further from equilibrium with its surroundings. This disequilibrium drives a diffusive flux that goes both up and down; the overlying mantle is warmer (lower solubility) but drier, while the colder deeper parts of the slab are colder (higher solubility) but equally hydrated. However, the back diffusion of water deeper into the slab causes water accumulation in the water concentration, leading a concentration peak which is even further out of equilibrium with overlying warm mantle.

Thus, the back-flux and accumulation of water in the slab drives an enhanced flux into the overlying mantle. Indeed, model calculations suggest that the water flux out of the slab is very weakly dependent on the temperature dependence of the solubility [*Richard, et al.*, 2006]. Moreover, given typical residence times of slabs floating horizontally across the transition-zone, for 50Myrs or more, essentially 50–100% of the water brought by entrainment into the transition-zone is expelled through this double-diffusive mechanism into the transition-zone. That it occurs over a relatively broad region (the extent of slab deflection) allows for enhanced distribution of water through the transition-zone.

Diffusion is important for removing water from the slab itself. However, small-scale chemically driven convection of hydrated material is also likely an important recirculating mechanism [*Bercovici and Karato*, 2003; *Leahy and Bercovici*, 2006]. Hydrated material entrained in the vertical downwelling would not only impede the downwelling, but could lead to small-scale instabilities. Moreover, warm mantle material overlying a flat, floating slab would also become buoyant when hydrated by the slab, and thus would likely become unstable. Hydrated material from the viscous-entrainment zone that is advected horizontally by a deflected floating slab would also lead to a relatively broad region of convectively unstable material. Rising chemically buoyant material may exhibit complex circulation patterns if it is stirred by the background mantle flow. Eventually, these buoyant anomalies would pass through the 410km boundary, whereupon they would undergo partial melting and return their water to the water-filter melt layer. The details of this convectively enhance water circulation have, however, yet to be explored.

Convection and Heat Source Distribution

One of the predictions of the water-filter model, even with the most recent adjustments discussed in previous sections, is that the heat-source distribution would be almost entirely confined to the sub-410km mantle. However, [*Bercovici and Karato*, 2003] conjectured that large-scale, whole mantle flow would be largely unaffected by such a layered, inhomogeneous heat-source distribution as long as there are no internal boundaries impermeable to the bulk flow. This hypothesis was tested in a two-dimensional isoviscous convection model by *Leahy and Bercovici* [2004] for a suite of possible heat-source distributions ranging from uniform whole-mantle heating, mantle heated uniformly only below 410km, to the extreme case of heating confined entirely to the transition-zone (under the assumption that radiogenic elements follow the water circulation through the transition-zone). These cases were also combined in various proportions with each other as well as with the contribution from secular cooling (which effectively acts as a uniform heat source). Stability and numerical results indicate that in almost every possible heating distribution, the large scale flow is almost completely unaffected by layered heating (Fig. 7). In only one end-member case, in which all possible heating was confined to the transition-zone, was circulation affected; however, even in this situation, while thermal anomalies were concentrated in the upper-most mantle, circulation still extended throughout the entire mantle (Fig. 7, see case 3). The addition of even minimal secular cooling in the mantle or some contribution from broadly distributed heating restores both the thermal anomalies and circulation to a whole-mantle configuration.

4. GEOPHYSICAL AND GEOCHEMICAL CONSEQUENCES

One of the most important predictions of the water-filter model is that there should be a discontinuous jump in the concentrations of incompatible elements at 410-km, although the major (compatible element) abundance should be nearly continuous. The model also predicts large lateral variation in the concentrations of incompatible elements such as hydrogen. Consequently, a useful test is to see if there are any geophysical observables that carry information on the spatial distribution of concentration of incompatible elements. Because of the relatively small concentrations, the concentrations of incompatible elements are difficult to infer from geophysical observations, except for hydrogen. Geophysically observable properties that are potentially sensitive to water (hydrogen) content include electrical conductivity and seismic wave velocities (and attenuation). In these studies, one needs to have high-resolution geophysical data sets and the relationships between water content and physical properties. Particularly critical is to establish the relationships between water content and physical properties based on laboratory data and theoretical models. This topic has recently reviewed by [*Karato*, 2003; 2006a; c].

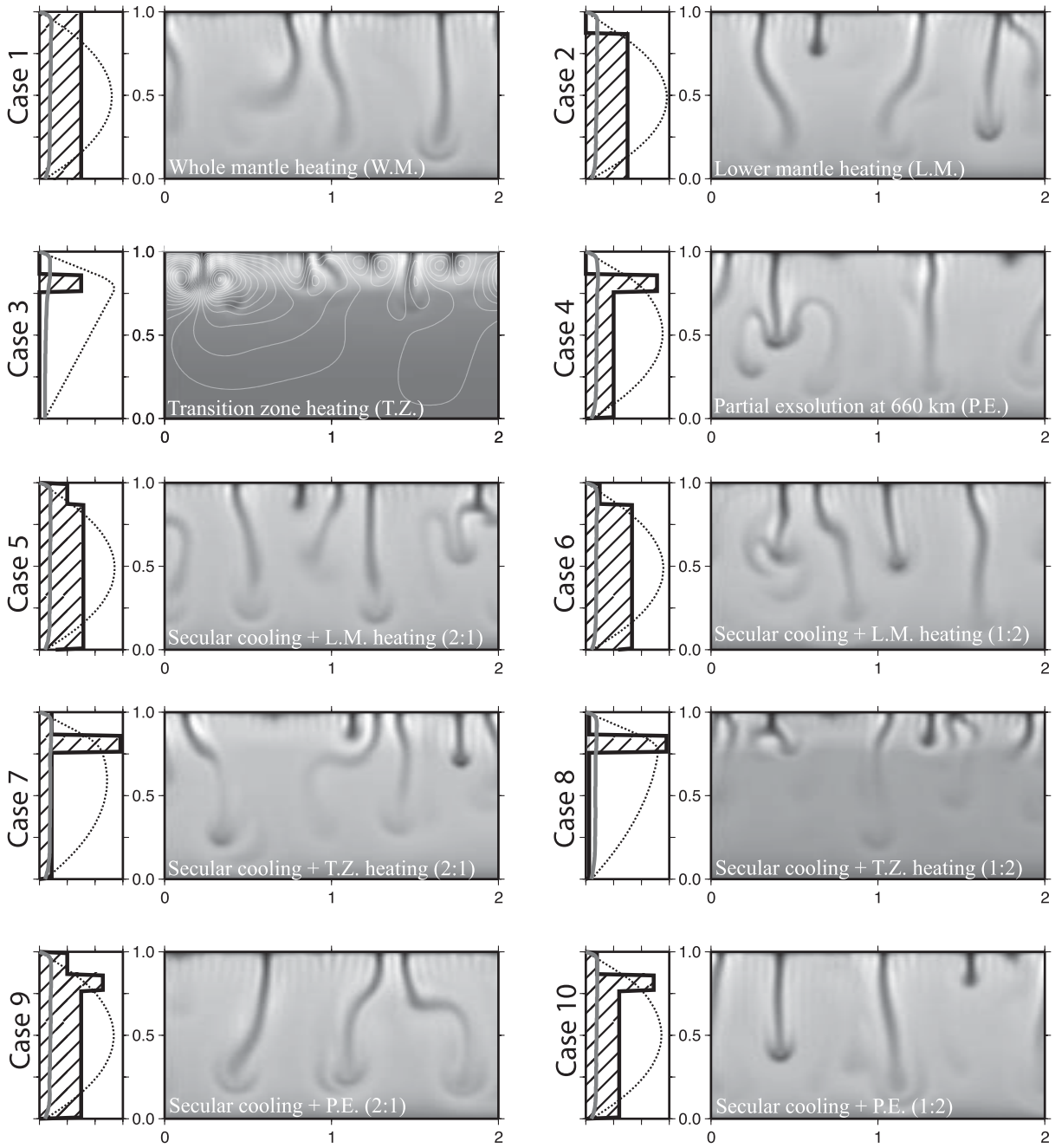

Fig. 7. Convection experiments: Temperature field and heating distributions for the 10 cases labeled. For each case, the left frame gives the heating distribution (shaded area) and the horizontally averaged temperature (dashed line). The right frame for each case is the total temperature field, where white represents hot regions and black represents cold regions. In case 3, stream lines have been added to demonstrate the whole region participates in the convective cycle even though the lower layer appears stable (after [*Leahy and Bercovici*, 2004]).

The TZWF model predicts a contrast in hydrogen (water) and other incompatible element concentrations between the upper mantle and the mantle below 410-km. If material circulation across the 410-km discontinuity is continuous without melting, then the concentrations of incompatible elements such as hydrogen must be the same between these two layers. A comparison of geophysically inferred electrical conductivity profile with the recent experimental data on the influence of water (hydrogen) content on electrical conductivity in wadsleyite and olivine shows that there is a marked contrast in water content across the 410-km. [*Huang, et al.*, 2005] inferred water content from electrical conductivity to conclude ~0.1-0.2 wt%. [*Huang, et al.*, 2006] estimated the ratio of hydrogen content between the transition zone and the upper mantle to be ~10 times more water than a typical upper mantle (with a large regional variation). The results of this analysis are insensitive to the uncertainties in temperature estimate and it provides a strong support for the TZWF model.

Seismological observations have also been used to infer the water content. There are at least two issues that can be addressed from this approach. Studies in this category include those from the thickness of the 410- km ([*van der Meijde, et al*., 2003; *Wood,* 1995; *Smyth and Frost*, 2002]), and the simultaneous inversion of topography on the '410-km' discontinuity and the velocity anomalies in the transition zone ([*Blum and Shen*, 2004; *Suetsugu, et al*., 2006]). A difficulty in this approach is the uncertainties in the relationships between water content and seismological observables (for details see [*Karato*, 2006a; c]). The exact relationship between the thickness of the 410- km and the water content is subject to uncertainty due primarily to the uncertainties in the model of dissolution of hydrogen [*Karato*, 2006b, c]. The inference of water content from the joint inversion of the topography of the 410-km discontinuity (or the thickness of the transition zone) and the velocity anomalies in the transition zone can provide a strong constraint. This method utilizes the notion that the anomalies of seismic wave velocity and the topography of the discontinuity depend on anomalies in temperature and water content. Using such an approach, [*Blum and Shen*, 2004] inferred the water content in the transition-zone beneath Africa using the velocity anomalies and the anomalies of the depth of the discontinuity. They inferred ~0.1 wt%. Similarly, [*Suetsugu, et al*., 2006] used the anomalies of velocity and thickness of the transition-zone beneath western Pacific and inferred that water content varies with geological setting and regions in which old slabs subduct contains ~1 wt% water, but regions in which young slabs subduct has much smaller water content. Recent experimental studies of elastic wave velocities in OH-bearing minerals at high pressure indicates that water has a much stronger influence on *S*-velocities than *P*-velocities, so that regions with "normal" *P*-velocities associated with high V_P/V_S ratios (resulting from low V_S) may be characteristic of hydration [see *Jacobsen and Smyth*, this volume].

There have been some reports suggesting the presence partial melt around 410-km (e.g., [*Revenaugh and Sipkin*, 1994; *Song, et al.*, 2004]). However, the direct connection between partial melting and the low velocities is not straightforward (e.g., [*Karato*, 2006c]) because regions of high melt fraction are expected to be highly localized, as suggested by theoretical modeling (e.g., see previous section and *Spiegelman and Elliott,* 1993]). A promising method to detect a thin melt-rich layer is to investigate seismological signals that are sensitive to the presence of a sharp impedance contrast (e.g., [*Chambers, et al.*, 2005]).

In addition to partial melting, spatial variation in hydrogen content will also have important effects on seismic wave velocities and attenuation [*Karato*, 2006c]. The TZWF model predicts that a broad region surrounding a subducting slab contains a large amount of enriched (hydrogen-rich) materials [*Leahy and Bercovici*, 2006] and hence will have low seismic wave velocities and high attenuation. *Obayashi et al.* [2006] reported low velocity anomalies in the transition zones ocean-side of the western Pacific subduction zone that is consistent with a model by *Leahy and Bercovici* [2006] (this model predicts hydrogen-rich regions in the *both sides* of a subducting slab. However, in the continental side, velocities will probably not be as low because it is on the colder top side of the slab (e.g., [*Fukao, et al*., 2001])).

Consequence for the Distribution of Trace Elements

One of the important contrasting geochemical characteristics between MORB and OIB is the generally higher concentrations of incompatible elements in OIB than MORB (Plate 3a). In more detail, the difference between MORB and OIB in terms of trace element abundance is larger for more incompatible elements. Also the degree of difference is large for certain regions of OIBs such as HIMU or EM-1 than OIB from Hawaii.

The TZWF model may explain important characteristics of trace element distribution patterns. Upon partial melting, those elements that have ionic radii and/or electrostatic charge that are largely different from the host ion in minerals tend to go to melt. One of the important conjectures in the TZWF model is that the MORB is produced by the partial melting of materials at shallow mantle that have already undergone "filtering" by partial melting at 410-km, while OIB is formed by partial melting at shallow mantle of materials that have not undergone filtering. Consequently, the MORB source materials are more depleted than the source

materials for OIB. Here we show a simple model calculation of trace element abundance based on a model that incorporates TZWF. We assume the following sequence of chemical differentiation. (i) The original chemical composition of Earth is chondritic. (ii) The chondritic material differentiated by the formation of continental crust. The chemical composition of residual materials can be calculated by mass balance by knowing the mass fraction of the continental crust (0.6 %). (iii) The residual materials will undergo transition-zone partial melting. Partial melting removes incompatible elements the degree to which this happens depends on the degree of melting and the partitioning coefficients. (iv) Materials that have undergone these two stages of differentiation will finally partially melt near the surface to form MORB. (v) Materials that have escaped differentiation in the transition-zone will undergo partial melting near the surface to form OIB.

In this calculation, we need to know the degree of melting, the partitioning coefficients of elements between melt and solid, and the mode of melting. The degree of melting for MORB is estimated to be ~10% based on the ratio of oceanic crust and residual lithosphere. The degree of melting for OIB is unknown, and we chose 1-5%. The degree of melting at 410-km depends on the mantle adiabat and the concentration of impurity components. The estimated impurity content in a typical Earth is ~1 wt% or less (Table 2), so we explored a range of degree of melting, 0.5-1.0%. The degree of melting at 410-km is important in assessing the effects of garnet on trace element abundance. Garnet has peculiar partition coefficients due to its flexible crystal structure: garnet has significantly higher partitioning coefficients for modestly compatible elements than other minerals. This garnet signature shows up, however, only for a large degree of melting, larger than a few percent. The partition coefficients are available only at modest pressures for melts without much volatiles [*Hauri, et al*., 1994]. *Taura et al.* [1998] investigated the influence of pressure on trace element partitioning, but the influence of pressure is only modest. *Wood and Blundy* [2002] estimated the influence of water on trace element partitioning, however, the indirect influence of water (through other physical property changes) in phases such as wadsleyite is unconstrained. Consequently we used the results by *Hauri, et al.* [1994] for element partitioning coefficients under low pressure and anhydrous conditions but assuming 30% of the material is garnet. A gross feature (relative incompatibility of various elements) of trace element distribution pattern is likely represented by the use of this set of partition coefficients, although some refinement will be needed when a better data become available.

The results are shown in Plate 3b. We note that we have reproduced the observed trace element abundance patterns for MORB and OIB (Hawaii) using the published partitioning coefficients and plausible degree of melting at 410-km and near the surface. In a classic model by *Hofmann* [1988], chemical evolution in Earth was assumed to have been caused by melting associated with the formation of continental and oceanic crust and subsequent melting at mid-ocean ridges but no melting is assumed at the deep mantle. Since the degree of melting at ~410-km is small, the transition-zone melting does not affect the trace element distribution pattern so much. In particular, the influence of garnet is not seen because the peculiar partition coefficients of trace elements in garnet (and melt) occur for relatively compatible elements such as Yb, Er and Lu for which the partition coefficients are ~10^{-1} and consequently, the "garnet signature" can be seen only after a high degree of melting (~10%). The trace element distribution patterns for more "enriched" OIB such as EM-1 or HIMU cannot be explained by our model. These regions require some additional processes for "enrichment" such as the involvement of continental lower crust and/or sediments.

Hydrogen is one of the highly incompatible elements whose partition coefficient is on the order of 10^{-3}, which is close to (or slightly smaller than) that of Rb. Consequently, if one assumes that Hawaii source regions are representative of deep mantle composition as argued above, then a contrast of hydrogen content between the upper mantle and the deep mantle will be similar to that of Rb, i.e., a factor of ~5 [*Hofmann*, 1997; 2004]. The inferred contrast in hydrogen content by [*Huang, et al*., 2006] is a factor of ~10 with a large regional variation. In other words, in order to create a factor of ~10 difference in hydrogen content between the upper mantle and the transition zone with the partition coefficient of water of $k=10^{-3}$, one needs ~1% melting for batch melting and ~0.2% for fractional melting. These values are in good agreement with what is expected from the concentration of volatile, incompatible elements and their partitioning coefficients. We therefore conclude that the observed concentrations of water in the upper mantle and the transition zone can be attributed to the filtering processes that occurs at ~410-km. Obviously, the filtering can be leaky as discussed before and consequently, we expect that the water content of the upper mantle is heterogeneous. If water content is significantly less than ~0.05wt%, then no melting occurs, and materials will go through the 410-km without filtering. If a material has large water content, say ~1 wt%, then the melt will be light and again filtering will not occur. These materials will form a localized upwelling to create OIB. If the water content of materials in the transition zone is in between these values, then the filtering will occur to change the water content to ~1/10 of the original value.

In contrast to the present analysis *Hirschmann et al.* [2005] argued that the TZWF model would predict a water content in the upper mantle that is too high compared to the inferred

values. They argued that if partial melting occurs at 410-km, then the upwelling materials will continue to melt and the upwelling materials (materials in the upper mantle) will have a water content higher than the inferred value of water in the source region of MORB (~0.01 wt%). The validity of such an argument hinges on the assumed values of partition coefficient of hydrogen and other thermochemical properties of minerals and melt that determine the degree of melting at a given P-T condition. There are large uncertainties in thermochemical properties of melts, but as we discussed above, plausible estimates of the partition coefficient (~10^{-3}) and the degree of melting (~1 %) give a reasonable value of water content in the upper mantle (~0.01 wt%).

Consequence for the Distribution of Isotopes

Contrasting geochemical characteristics between MORB and OIB include not only the abundance of trace elements but also the distribution of isotopes. For example, OIB has higher $\frac{^{87}Sr}{^{86}Sr}$ and $\frac{^{143}Nd}{^{144}Nd}$ than MORB. Also, the variation of these isotopic ratios is larger for OIB than for MORB (e.g., [*Hofmann*, 1997], see however [*Hofmann*, 2004] who emphasized the diversity of isotope and other geochemical data from MORB). Since melting does not change the isotopic compositions, the explanation of these characteristics must be sought for some indirect mechanisms. One obvious mechanism is the modification of the parent to daughter element abundance ratio by melting. Consider a radioactive decay, $^{\alpha}A \rightarrow {}^{\gamma}B$. If element B has another isotope, $^{\beta}B$, that is not created by radioactive decay, the isotopic ratio $\frac{[\gamma_B]}{[\beta_B]}$ will increase with time and with increasing concentration of element A, $\frac{[\gamma_B]}{[\beta_B]} = \left(\frac{[\gamma_B]}{[\beta_B]}\right)_0 + \frac{[\alpha_A]}{[\beta_B]}\left(e^{\frac{t}{\tau}} - 1\right)$ where τ is the half life-time of radioactive decay. If there are two regions (i.e., the OIB source region and the MORB source region) that contain different $\frac{[\gamma_B]}{[\beta_B]}$ and $\frac{[\alpha_A]}{[\beta_B]}$ ratios (but the same initial $\frac{[\gamma_B]}{[\beta_B]}$ then for a period of time t, $\Delta\frac{[\gamma_B]}{[\beta_B]} = \Delta\frac{[\alpha_A]}{[\beta_B]}\left(e^{\frac{t}{\tau}} - 1\right)$, where Δ represents a change in isotopic ratio over time t. We use this relation to calculate $\Delta\frac{[\alpha_A]}{[\beta_B]}$ from observed $\Delta\frac{[\gamma_B]}{[\beta_B]}$ and t/τ that is required by the model (τ ~0.5 Gys) and the half-life of the relevant radioactive scheme. Next we compare model Δ ratios with observed Δ ratios inferred from the difference in composition of "depleted" and "undepleted" mantle (e.g., [*Newsom*, 1995]).

Model and observed values of the isotopic ratios for Sr, Nd, Re/Os, and Pb are summarized in Fig. 8. The data on $\Delta\frac{[\gamma_B]}{[\beta_B]}$ are largely from [*Hofmann*, 1997], but additional data on Os are from [*Hauri and Hart*, 1993]. We conclude that the observed isotopic compositions of MORB and OIB are largely consistent with the TZWF model, although some of the "extreme" compositions such as EM-2 are difficult to explain by this model.

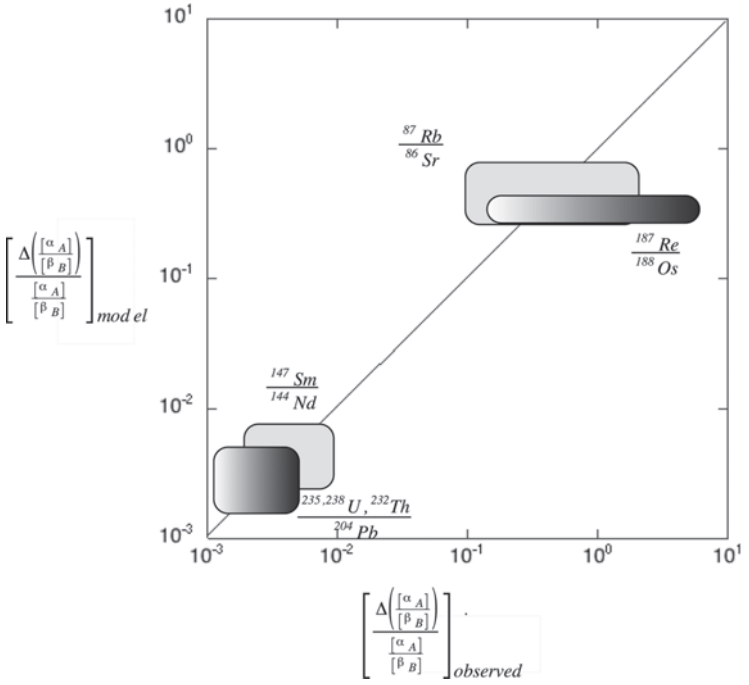

Fig. 8. Comparison of differences in isotopic ratios of radioactive isotope $^{\alpha}A$ to stable isotope $^{\beta}B$ created by partial melting at 410-km required to explain the geochemical observations by the TZWF model and the observed ratios.

It is often argued that the observed isotopic compositions are not consistent with a model in which the whole mantle was depleted at the time of continental crust formation (e.g., [*van Keken, et al.*, 2002]), and that more than 1 billion years are needed to establish the observed differences in isotopic compositions between MORB and OIB (e.g., [*Hofmann*, 1997]). We have shown that ~0.5 Gys of separation is long enough to result in most of the observed differences in isotopic ratios.

The observations on helium isotopic ratio are not straightforward to explain. Briefly, $\frac{[^3He]}{[^4He]}$ for OIB are much more scattered (and in general larger) than those of MORB. ^4He is a radiogenic isotope that is produced by the radioactive decay of ^{238}U or ^{232}Th. Consequently, if the TZWF operates well then the concentration of radioactive parent atoms such as ^{238}U or ^{232}Th will be lower in the upper mantle (MORB source region), and hence MORB would have a *higher* $\frac{[^3He]}{[^4He]}$ than OIB. We note that the observed $\frac{[^3He]}{[^4He]}$ may also be controlled by the degree of depletion of helium. [*Brooker, et al.*, 2003; *Parman, et al.*, 2005] reported that helium behaves like a highly incompatible element during partial melting (and diffusion of helium is very fast and hence distribution of *He* will always be in chemical equilibrium). The small reported partition coefficient (on the order of $\sim 10^{-3}$) leads to significant depletion in helium in the source region of MORB in our model, and hence the observed lower $\frac{[^3He]}{[^4He]}$ ratio for MORB can be due to the depletion of helium in the source region of MORB. Similarly, *Ar* and other rare gas elements are likely sequestered into the deep mantle due to their low partition coefficients ([*Brooker, et al.*, 2003]) (and relatively high diffusion coefficients [*Harrison*, 1981]), if TZWF operates. This provides a simple explanation for the *Ar* paradox (i.e., there are too much *Ar* in the atmosphere compared to the amount of *K* in the upper mantle; [*Allègre, et al.*, 1996]).

In examining these models incorporating partial melting and element partitioning, an important implicit assumption is chemical equilibrium. This assumption is not secure for elements with very small diffusion coefficients. The chemical equilibrium will be attained if the time scale of reaction exceeds $t > \frac{d^2}{\pi^2 D}$ where d is grain-size (~ 3 mm) and D is relevant diffusion coefficient. The diffusion coefficients vary from one species to another (see Table 3), but from the Table 3 with t ~10 My, chemical equilibrium is certainly attained for *He, Pb*, and presumably for *Sr* and *Sm*, but the distribution of *U* and *Th* is likely out of equilibrium. *U* and *Th* likely behave like compatible elements, but *He* is a highly incompatible element, and therefore if there is melting at ~410-km, much of *U* and *Th* will be transported to the upper mantle but not much of *He*. This explains the helium paradox, i.e., the amount of *He* flux is too much smaller than expected from the amount of *U* and *Th* [*O'Nions and Oxburgh*, 1983].

Table 3. Diffusion coefficients of some trace elements in typical minerals (cpx, olivine) at $\frac{T}{T_m} \sim 0.7$ (T_m is the melting temperature of the mineral)

U, Th	(cpx)	$\sim 10^{-20}$ m^2/s	[*Van Orman, et al.*, 1998]
Pb	(cpx)	$\sim 10^{-16}$	[*Cherniak*, 1998]
Sr, Sm	(cpx)	$\sim 10^{-18}$	[*Sneeringer, et al.*, 1984]
He	(ol)	$\sim 10^{-11}$	[*Hart*, 1984]

The overall processes of geochemical cycling in this model are summarized in Plate 4 in which processes associated with upwelling currents are emphasized**.** A unique feature of this model, as compared to any previous models, is the role of (a small amount of) melting at ~410-km caused by the presence of volatile components H_2O, CO_2, Na_2O, K_2O. We have shown that melting at this depth is highly likely and that the melt thus formed has a higher density than the surrounding minerals under some conditions. We propose that if the volumetrically dominant part of the deep mantle is made of relatively depleted materials such as the source region of Hawaii or FOZO (after the formation of continental crust), together with volumetrically minor more enriched materials, then almost all geochemical observations can be explained naturally as the result of melting at ~410-km without violating the geophysical constraints suggesting whole mantle wide convection. They include trace element abundance patterns, isotopic ratios, abundance of *He* relative to *U* and *Th* (the helium/heat paradox), and the abundance of *Ar* relative to the abundance of *K, U* and *Th* (the *Ar* paradox). The homogeneity of composition of MORB compared to that of OIB is partly attributed to the dominance of Hawaii (or FOZO) type composition of the deep mantle, and some homogenization due to melting.

Homogeneity of MORB may also be due to the selective filtering: filtering to form MORB source materials occurs only for materials with certain composition as discussed in the previous section. The TZWF acts as a "low-pass" filter through which only materials with relatively depleted character passes into the MORB source region. OIB may also be formed when a hot plume goes through the transition zone that has a material typical of the deep mantle (Hawaii type composition, by assumption). These hot materials will escape TZWF if their upwelling velocity is faster than the velocity of lateral flow of a melt layer and/or when the melt density is lighter than the surrounding materials due to high temperature as discussed by [*Bercovici and Karato*, 2003].

The source region of OIB is considered to occupy a large fraction of mantle (e.g, [*Albarède and van der Hilst*, 2002; *Allègre*, 1997]). In almost all previous models, the source regions for MORB and OIB are assumed to have been isolated for billions of years and the geodynamic difficulty is

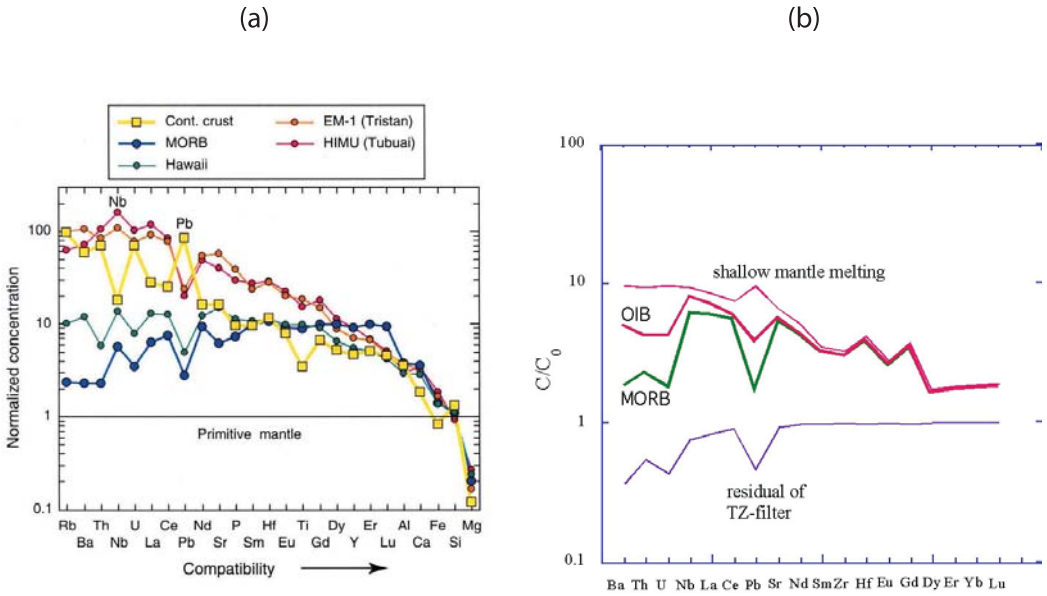

Plate 3. A comparison of (a) the observed trace element abundance pattern (from [*Hofmann*, 1997]) with (b) the results of model calculations. "Residual of TZ-filter" shows the pattern of trace element concentration after the TZWF. The MORB trace element distribution pattern reflects this pattern but involves another high-degree melting at the surface. The OIB distribution pattern does not include the influence of TZWF. The difference between OIB and MORB is either TZWF operates or not.

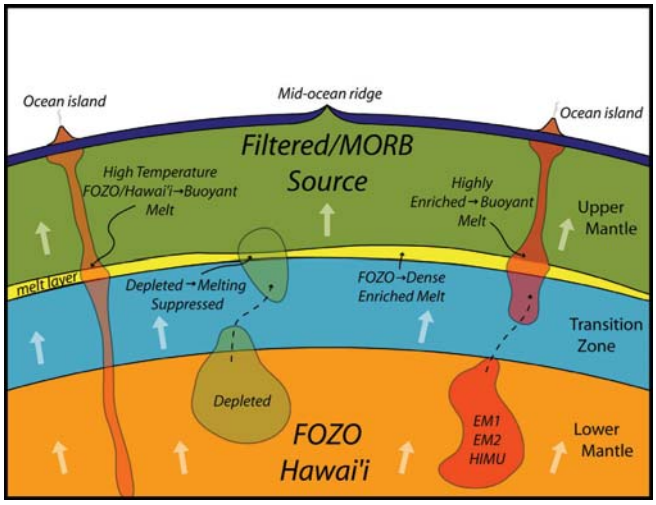

Plate 4. Cartoon showing roles of transition-zone melting on the geochemical cycling in Earth's mantle. The majority of the mantle was assumed to be made of the residual materials after the formation of continental crust (Hawaii or FOZO type composition). These materials are moderately depleted, and will melt, assisted by volatiles such as water, when they move across the 410-km boundary from below to form a dense melt. Much of the incompatible elements will be removed from the upwelling materials and the resultant depleted materials will become the source materials for MORB. Highly enriched materials such as EM-1 will be melted, but the density of these melt is likely low because of high concentration of water (or because of high temperature). These enriched materials will remain enriched as they ascend and will form enriched OIB. Relatively depleted OIB can also be formed when a hot plume goes through the transition zone. In such a case, melting occurs at ~410-km, but the melt will be less dense because of a high temperature, and hence the melt rises to form a OIB with relatively depleted signature. Highly depleted materials in the deep mantle will not undergo melting and will directly be transported to the upper mantle to become a source material for MORB. When a dense melt is formed, then the transition-zone melting will sequester highly incompatible elements into the deeper mantle including *He* and *Ar* (but not *U* and *Th* that have very low diffusion coefficients). This model provides a unified explanation for a broad range of geochemical observations without violating geophysical constraints that mantle convection occurs more-or-less in the whole mantle wide flow.

to reconcile such a model with geodynamic observations suggesting whole mantle convection. Although our model does not exclude the presence of a relatively small amount of materials that have been isolated for billions of years, we propose that there is an additional process that may have an important consequence on geochemical cycling.

We note that the proposed partial melting has an important effect on the distribution of "impurities" such as hydrogen and potassium. All incompatible elements will be sequestered in the deep mantle if the TZWF were to occur. The transition zone and the lower mantle will have a higher hydrogen content than the upper mantle, which will result in a lower viscosity in these regions than in the case of homogeneous composition. Similarly, much of the radioactive elements such as potassium and uranium will also be sequestered in the deep mantle. Inference of the composition of the mantle from upper mantle rocks (e.g., [*McDonough and Sun*, 1995]) will lead some bias for highly incompatible elements.

5. SUMMARY AND PERSPECTIVES

We have presented a review and refinement of the TZWF model originally proposed by *Bercovici and Karato* [2003]. Mineral physics observations suggest that a small degree of partial melting at around 410-km discontinuity is likely under a broad range of conditions, but results in a dense (denser than upper mantle minerals but lighter than transition zone minerals) melt for relatively low concentrations of hydrogen (water), whereas flux melting due to higher concentrations of water results in a light (buoyant) melt. This melting in the transition-zone can modify the distribution of highly incompatible elements without affecting the distribution of relatively compatible elements and thus provides an explanation for a broad range of geochemical observations. conditions for creating a dense melt is difficult at this stage due mainly to the limited knowledge about the role of CO_2, K_2O and Na_2O as well as H_2O in melting and the melt density under transition zone conditions and represents an experimental area ripe for exploration.

We have also reviewed recent observational constraints of this model. A combination of geodynamic modeling and mineral physics suggests several features that are characteristic to the TZWF model. Obviously, any evidence for a melt-rich layer at ~410-km will support the model, but we note formidable challenges in detection of such a layer because even partial melt beneath some mid-ocean ridges has not been well resolved by seismological observations ([*Wolfe and Silver*, 1998]). Because partial melt is probably highly localized, seismological detection of a thin (partially) molten layer will require a high-resolution technique that is sensitive to the impedance contrast (e.g., [*Chambers, et al.*, 2005]). Although indirect, the distribution of hydrogen can provide important data to test the model. Hydrogen distribution can be broad in some cases and hydrogen has strong influence on some geophysically measurable properties such as electrical conductivity and seismic wave velocity and attenuation. One important observation is the jump in electrical conductivity at ~410-km in many regions that suggest a jump in hydrogen content which is consistent with the TZWF model. The TZWF model also predicts that the distribution of hydrogen (and other volatile elements) is laterally heterogeneous. Recent seismological and electrical conductivity observations support this notion (e.g., [*Fukao, et al.*, 2004; *Obayashi, et al.*, 2006; *Suetsugu, et al.*, 2006]). However, much remain poorly constrained and further progress in the following areas is needed: (i) the relationship between geophysical observations (seismic wave velocities and attenuation, electrical conductivity) and water content or partial melting needs to be better constrained, and (ii) more detailed geophysical exploration is needed to map the distribution of hydrogen, and melting in the mantle (for a review see [*Karato*, 2006c]).

In addition, geochemical consequence of the model needs to be explored in more detail. Improved determination of partition coefficients of trace elements between minerals and a volatile-rich melt under the deep mantle conditions is required. The present model has far-reaching implications for the chemical evolution and the volcanism in Earth, but detailed prediction of geochemical consequences is difficult due mainly to the lack of experimental data on element partitioning at deep mantle conditions. The model implies that the mantle is likely layered with respect to highly incompatible elements such as hydrogen, carbon, potassium and sodium.

Acknowledgements. We thank Rajdeep Dasgupta, Marc Hirschmann, Steve Jacobsen, and Joe Smyth for sending us their papers or experimental data prior to publication, and Eiji Ohtani and Jay Ague for discussion. Persistent criticisms on the TZWF model by Marc Hirschmann helped improve the paper. Editorial comments by Steve Jacobsen and Susan van der Lee helped clarify the presentation. This research is supported by National Science Foundation.

APPENDIX I: SIMPLE DECOMPACTION THEORY FOR A HEAVY MELT LAYER

To examine decompaction of the heavy melt layer, we employ the generalized two-phase damage equations [*Bercovici et al.*, 2001a,b; *Ricard et al.*, 2001; *Bercovici and Ricard*, 2003; *Ricard and Bercovici*, 2003; *Bercovici and Ricard*, 2005], which we only briefly summarize in order to

develop our decompaction scaling relationships. We note in advance that in the following equations, subscripts *f* and *m* refer to fluid (i.e., the melt phase) and matrix (i.e., the solid phase) phases, respectively. The conservation of mass equations in two-phase theories [*McKenzie*, 1984; *Bercovici et al.*, 2001a] are

$$\frac{\partial \phi}{\partial t} + \boldsymbol{\nabla} \cdot [\phi \mathbf{v}_f] = 0 \tag{A1-1}$$

$$\frac{\partial (1-\phi)}{\partial t} + \boldsymbol{\nabla} \cdot [(1-\phi)\mathbf{v}_m] = 0, \tag{A1-2}$$

where ϕ is porosity, and $\mathbf{v}_f$ and and $\mathbf{v}_m$ are the fluid and matrix velocities. We assume steady state and that while the solid matrix undergoes 1D vertical de- compaction, the fluid undergoes 2D flow as slab entrainment enforces horizontal drainage of the melt. Thus, we obtain

$$\frac{\partial}{\partial z}[(1-\phi)w_m] = 0 \tag{A1-3}$$

$$\frac{\partial \phi w_f}{\partial z} + \frac{\partial \phi u_f}{\partial x} = 0 \tag{A1-4}$$

where w_j and u_j are the vertical and horizontal velocity components, respectively, of phase *j*. We assume that the solid mantle below the 410km boundary is up- welling at constant velocity *W* and upon crossing the boundary undergoes melting by a fraction *f* ; we assume that melt and solid densities are nearly the same and thus neglect the density difference $\Delta\rho = \rho_m - \rho_f$ unless, as prescribed by the Boussineseq approximation, it is multiplied by gravity *g*; thus we make no distinction between *f* being a mass or volume fraction. As solid flow is only one- dimensional the vertical solid flux crossing the 410km boundary never changes and thus integration of (A1-3) yields

$$(1-\phi)w_m = (1-f)W \quad \text{or} \quad w_m = \frac{1-f}{1-\phi}W \tag{A1-5}$$

We assume for simplicity that the horizontal entrainment rate is given by a constant $\partial uf/\partial x = U$ which approximates the steady accumulation of melt with horizontal distance from the center of the upwelling; thus (A1-4) becomes

$$\frac{\partial \phi w_f}{\partial z} = -\phi U \tag{A1-6}$$

where we assume ϕ is only a function of *z*. The initial melt fraction or porosity at $z = 0$ is simply *f* and the input melt flux is *fW*. Because the melt is heavy it will first accumulate into a high porosity region; however, the horizontal melt entrainment will eventually drain away all the melt so that at some height $z = H$ we get $\phi = 0$. Therefore, if we integrate (A1-6) from $z = 0$ to $z = H$, with the boundary conditions that $\phi wf = fW$ at $z = 0$, and $wf = 0$ at $z = H$, we obtain

$$fW = U\int_0^H \phi(z)dz = UH\Theta \tag{A1-7}$$

where of course $\Theta = \frac{1}{H}\int_0^H \phi dz$.

We will also be concerned with terms in the momentum equation proportional to the velocity difference $\Delta w = w_m - w_f$ and for this we can add (A1-3) and (A1-6) to obtain

$$\frac{\partial \phi \Delta w}{\partial z} = \frac{\partial w_m}{\partial z} + \phi U \tag{A1-8}$$

The momentum equations for each phase (assuming the melt is much less viscous than the solid) are

$$0 = -\phi\left[\boldsymbol{\nabla} P_f + \rho_f g\hat{\mathbf{z}}\right] + c\Delta\mathbf{v} \tag{A1-9}$$

$$0 = -(1-\phi)\left[\boldsymbol{\nabla} P_m + \rho_m g\hat{\mathbf{z}}\right] + \boldsymbol{\nabla}\cdot[(1-\phi)\underline{\boldsymbol{\tau}}_m] - c\Delta\mathbf{v} + \Delta P\boldsymbol{\nabla}\phi \tag{A1-10}$$

where *g* is gravity, $\Delta\mathbf{v} = \mathrm{v}m - \mathrm{v}f$, and *c* is the coefficient for viscous drag between phases, also referred to as the Darcy drag coefficient, and as is typically $c = \mu_f/k$ where μ_f is fluid melt viscosity and *k* is a reference permeability [*McKenzie*, 1984; *Bercovici et al.*, 2001a]; P_j and ρ_j are the pressure and density, respectively, in phase *j* and the density of each phase is assumed constant. The deviatoric stress for the solid phase is given by

$$\underline{\boldsymbol{\tau}}_m = \mu_m\left[\boldsymbol{\nabla}\mathbf{v}_m + [\boldsymbol{\nabla}\mathbf{v}_m]^t - \frac{2}{3}(\boldsymbol{\nabla}\cdot\mathbf{v}_m)\underline{\mathbf{I}}\right] \tag{A1-11}$$

where μ_m is solid matrix viscosity. The pressure difference $\Delta P = P_m - P_f$ in the absence of surface tension and strongly nonequilibrium effects (such as damage) is

$$\Delta P = -\frac{K\mu_m}{\phi}\boldsymbol{\nabla}\cdot\mathbf{v}_m \tag{A1-12}$$

where $K \approx 1$. The momentum equations are combined by taking ϕ times (A1-10) minus $1-\phi$ times (A1-9); we also substitute (A1-12), and keep only the vertical component, thereby obtaining

$$0 = \mu_m\frac{\partial}{\partial z}\left((1-\phi)\left(\frac{4}{3}+\frac{1}{\phi}\right)\frac{\partial w_m}{\partial z}\right) - (1-\phi)\Delta\rho g - c\Delta w/\phi \tag{A1-13}$$

which is the standard 1D compaction equation. We further multiply (A1-13) by ϕ^2, take the derivative of the resulting equation with respect to *z*, and eliminate both w_m, using (A1-5), and Δw, using (A1-8):

$$\begin{aligned} 0 =& \mu_m W(1-f)\frac{\partial}{\partial z}\left[\phi^2\frac{\partial}{\partial z}\left((1-\phi)\left(\frac{4}{3}+\frac{1}{\phi}\right)\frac{\partial}{\partial z}\frac{1}{1-\phi}\right)\right] \\ &- \Delta\rho g\frac{\partial}{\partial z}(\phi^2(1-\phi)) - c\left(W(1-f)\frac{\partial}{\partial z}\frac{1}{1-\phi} + U\phi\right) \end{aligned} \tag{A1-14}$$

We can nondimensionalize the above equation by writing $z = \delta z'$, $c = \mu_m \delta^2$, $U = (W/\delta)U'$ and $\Delta\rho g = -(\mu_m W/\delta^2)\beta$ where $\delta = \sqrt{\mu_m/c}$ is the compaction length and $\beta > 0$ is the dimensionless melt "heaviness" (note that with a heavy melt $\Delta\rho = \rho_m - \rho_f < 0$); we thus obtain

$$0 = (1-f)\frac{\partial}{\partial z'}\left[\phi^2 \frac{\partial}{\partial z'}\left((1-\phi)\left(\frac{4}{3}+\frac{1}{\phi}\right)\frac{\partial}{\partial z'}\frac{1}{1-\phi}\right)\right] + \beta\frac{\partial}{\partial z'}(\phi^2(1-\phi)) - (1-f)\frac{\partial}{\partial z'}\frac{1}{1-\phi} - U'\phi \quad \text{(A1-15)}$$

We can develop a scaling analysis to (A1-15) by using a trial function for ϕ that has the right symmetry and boundary conditions. To leading order, $\phi(z')$ can be assumed a parabolic function wherein

$$\phi(z') = \Phi - (\Phi - f)\left(\frac{z'}{H'}\left(1+\sqrt{\frac{\Phi}{\Phi - f}}\right) - 1\right)^2 \quad \text{(A1-16)}$$

where we require that $\phi = f$ at $z' = 0$ and $\phi = 0$ at $z' = H'$ where $H' = H/\delta$. Moreover, with this nondimensionalization and the assumed form of $\phi(z')$, (A1-7) yields $f = U' H' \Theta$ where

$$\Theta = \Phi - \frac{1}{3}\frac{\Phi^{3/2} + (\Phi - f)^{3/2}}{\Phi^{1/2} + (\Phi - f)^{1/2}} \quad \text{(A1-17)}$$

For the scaling analysis, we evaluate the amplitude of the terms in (A1-15) by integrating it from $z' = 0$ to H', employing both (A1-16) and (A1-7), and make the reasonable assumption that $f \ll 1$; assuming the resulting viscous resistance terms balance the gravitational settling term, we obtain (after considerable algebra) an implicit scaling relationship for Φ as a function of U (i.e., by writing the function $U(\Phi)$), which we express in dimensional form:

$$U = \sqrt{\frac{W|\Delta\rho|g}{2\mu_m}}\frac{f\sqrt{f}}{\Theta\left(\sqrt{\Phi} + \sqrt{\Phi - f}\right)} \quad \text{(A1-18)}$$

Since $H' = f/(U'\Theta)$ or $H = f W/(U\Theta)$ we also have a relationship for the melt layer thickness (again, in dimensional form)

$$H = \sqrt{\frac{2\mu_m W}{|\Delta\rho|g}}\frac{\left(\sqrt{\Phi} + \sqrt{\Phi - f}\right)}{\sqrt{f}} \quad \text{(A1-19)}$$

Equations (A1-18) and (A1-19) are used to construct Figure 3 for which we consider a full of possible entrainment rates U.

APPENDIX II.

Some Notes on the Temperature (and Pressure) Dependence of Hydrogen Solubility

There is some confusion in the literature on the issues of temperature and pressure dependence of solubility of hydrogen (or another volatile species). The solubility is defined by the reaction between a volatile phase and a solid, viz.,

$$fluid + solid \Leftrightarrow solid \cdot volatile \quad \text{(A2-1)}$$

where fluid could be water, and $solid \cdot volatile$ denotes a solid that contains volatile element (such as hydrogen). For example, in case of the reaction between water and wadsleyite (or olivine), the dominant reaction is given by

$$H_2O + mineral \Leftrightarrow (2H)_M^{\times} + O_O^{\times} + MgO_{surface} \quad \text{(A2-2)}$$

where $(2H)_M^{\times}$ is a point defect that contains two protons at M-site, $O_O^{\times}$ is an oxygen ion at O-site. Applying the law of mass action to reaction (A2-2), one obtains,

$$\left[(2H)_M^{\times}\right] \propto f_{H2O}(P,T)\cdot \exp\left(-\frac{\Delta u + P\Delta v}{RT}\right)\cdot a_{MgO}^{-1} \quad \text{(A2-3)}$$

where $\left[(2H)_M^{\times}\right]$ is the concentration of $(2H)_M^{\times}$, $f_{H2O}(P,T)$ is the fugacity of water, $\Delta u, \Delta v$ are the difference in internal energy and volume associated with reaction (A2-2). The solubility of hydrogen depends on T and P through $f_{H2O}(P,T)$ and $\exp\left(-\frac{\Delta u}{RT}\right)$ terms. Note that the water fugacity is in general a strong function of P and T. This is true for pure water as well as for a case where water forms solution with a silicate melt. For pure water, the fugacity of water at high P and T (P~5-15 GPa, T~1000-2000 K) is approximately an exponential function of P and T, $f_{H2O}(P,T) \propto exp\left(\frac{H_{H2O}}{RT}\right) = exp\left(\frac{E_{H2O}+PV_{H2O}}{RT}\right)$ with $v_{H2O} \approx 11 \times 10^{-6}$ m^3/mol (~molar volume of water at P~5-15 GPa) and $E_{H2O} \approx 0$ kJ/mol ($H_{H2O} = E_{H2O} + PV_{H2O} \approx$ 110 kJ/mol). This means that if one observes very small pressure dependence at relatively low temperatures where free water exists (this is what [*Demouchy, et al.*, 2005] reported), then the volume change of the system should be $\Delta v \sim 11\ 10^{-6}$ m^3/mol rather than ~0 m^3/mol as argued by [*Demouchy, et al.*, 2005] (note that the conclusion by [*Demouchy, et al.*, 2005] would be inconsistent with the above defect model (equation (A2-2)) but $\Delta v \sim 11\times10^{-6}$ m^3/mol is exactly what the model (A2-2) would imply). Similarly, the observed weak temperature dependence of hydrogen solubility at relatively low temperatures implies that $\Delta h \equiv \Delta u + P\Delta v \approx 100$ kJ/mol at P~10-13 GPa. Obviously, when water is present in the silicate melt, then its fugacity will be lower, and as the silicate fraction increases (with temperature), its fugacity decreases.

REFERENCES

Agee, C. B., and D. Walker (1988), Static compression and olivine flotation in ultrabasic silicate liquid, *Journal of Geophysical Research*, *93*, 3437–3449.

Albarède, F., and R. D. van der Hilst (2002), Zoned mantle convection, *Philosophical Transactions of Royal Society of London*, *A360*, 2569–2592.

Allègre, C. J. (1997), Limitation on the mass exchange between the upper and the lower mantle: the evolving convection regime of the Earth, *Earth and Planetary Science Letters*, *150*, 1–6.

Allègre, C. J., et al. (1996), The argon constraints on mantle structure, *Geophysical Research Letters*, *23*, 3555–3557.

Aubaud, C., et al. (2006), Intercalibration of FTIR and SIMS for hydrogen measurements in glasses and nominally anhydrous minerals, *American Mineralogist*, submitted.

Bell, D. R., et al. (2003), Hydroxide in olivine: A quantitative determination of the absolute amount and calibration of the IR spectrum, *Journal of Geophysical Research*, *108*, 10.1029/2001JB000679.

Bercovici, D., and S. Karato (2003), Whole mantle convection and transition-zone water filter, *Nature*, *425*, 39–44.

Bercovici, D., and Y. Ricard (2003), Energetics of two-phase model of lithospheric damage, shear localization and plate-boundary formation, *Geophysical Journal International*, *152*, 1–16.

Bercovici, D., et al. (2001), A two-phase model for compaction and damage 1. General theory, *Journal of Geophysical Research*, *106*, 8887–8906.

Blum, J., and Y. Shen (2004), Thermal, hydrous, and mechanical states of the mantle transition zone beneath southern Africa, *Earth and Planetary Science Letters*, *217*, 367–378.

Bolfan-Casanova, N. (2005), Water in the Earth's mantle, *Mineralogical Magazine*, *69*, 229–257.

Brooker, R. A., et al. (2003), The 'zero charge' partitioning behaviour of noble gases during mantle melting, *Nature*, *423*, 738–741.

Chambers, K., et al. (2005), Reflectivity of the 410-km discontinuity from PP and SS precursors, *Journal of Geophysical Research*, *110*, 10.1029/2004JB003345.

Cherniak, D. J. (1998), Pb diffusion in clinopyroxene, *Chemical Geology*, *150*, 105–117.

Dasgupta, R., and M. M. Hirschmann (2006), Deep melting in the Earth's upper mantle caused by CO_2, *Nature*, *440*, 659–662.

Demouchy, S., et al. (2005), Pressure and temperature-dependence of water solubility in iron-free wadsleyite, *American Mineralogist*, *90*, 1084–1091.

Frost, D. J., and B. J. Wood (1997), Experimental measurements of the properties of H_2O-CO_2 mixtures at high pressures and temperatures, *Geochimica et Cosmochimica Acta*, *61*, 3301–3309.

Fukao, Y., et al. (2004), Trans-Pacific temperature field in the mantle transition region derived from seismic and electromagnetic tomography, *Earth and Planetary Science Letters*, *217*, 425–434.

Fukao, Y., et al. (1992), Subducting slabs stagnant in the mantle transition zone, *Journal of Geophysical Research*, *97*, 4809–4822.

Fukao, Y., et al. (2001), Stagnant slabs in the upper and lower mantle transition zone, *Review of Geophysics*, *39*, 291–323.

Gasparik, T. (1993), The role of volatiles in the transition zone, *Journal of Geophysical Research*, *98*, 4287–4299.

Grand, S. (1994), Mantle shear structure beneath Americas and surrounding oceans, *Journal of Geophysical Research*, *99*, 11591–11621.

Hae, R., et al. (2006), Hydrogen diffusivity in wadelyite and water distribution in the mantle transition zone, *Earth and Planetary Science Letters*, *243*, 141–148.

Harrison, T. M. (1981), Diffusion of ^{40}Ar in hornblende, *Contributions to Mineralogy and Petrology*, *78*, 324–331.

Hart, S. R. (1984), He diffusion in olivine, *Earth and Planetary Science Letters*, *70*, 297–302.

Hauri, E. H., and S. R. Hart (1993), Re-Os isotope systematics of HIMU and EMII oceanic basalts from the south Pacific Ocean, *Earth and Planetary Science Letters*, *114*, 353–371.

Hauri, E. H., et al. (1994), Experimental and natural partitioning of Th, U, Pb and other trace elements between garnet, clinopyroxene and basaltic melt, *Chemical Geology*, *117*, 149–166.

Hirschmann, M. M. (2006), Petrologic structure of a hydrous 410 km discontinuity, in *Earth's Deep Water Cycle*, edited by S. D. Jacobsen and S. van der Lee, American Geophysical Union, Washington DC.

Hirschmann, M. M., et al. (2005), Storage capacity of H_2O in nominally anhydrous minerals in the upper mantle, *Earth and Planetary Science Letters*, *236*, 167–181.

Hirschmann, M. M., et al. (1998), The effect of alkalis on the silica content of mantle-derived melts, *Geochimica et Cosmochimica Acta*, *62*, 883–902.

Hofmann, A. W. (1988), Chemical differentiation of the Earth: the relationship between mantle, continental crust, and oceanic crust, *Earth and Planetary Science Letters*, *90*, 297–314.

Hofmann, A. W. (1997), Mantle geochemistry: the message from oceanic volcanism, *Nature*, *385*, 219–228.

Ito, E., and T. Katsura (1989), A temperature profile of the mantle transition zone, Hofmann, A. W. (2004), Sampling mantle heterogeneity through oceanic basalts: isotopes and trace elements, in *Treatise on Geochemistry*, edited by H. D. Holland and K. K. Turekian, pp. 61–101, Elsevier, Amsterdam.

Huang, X., et al. (2005), Water content of the mantle transition zone from the electrical conductivity of wadsleyite and ringwoodite, *Nature*, *434*, 746–749.

Huang, X., et al. (2006), A wet mantle conductor? (Reply), *Nature*, *439*, E3–E4.

Inoue, T. (1994), Effect of water on melting phase relations and melt composition in the system Mg_2SiO_4-$MgSiO_3$-H_2O up to 15 GPa, *Physics of Earth and Planetary Interiors*, *85*, 237–263.

Inoue, T., and H. Sawamoto (1992), High pressure melting of pyrolite under hydrous condition and its geophysical implications, in *High-Pressure Research: Application to Earth and Planetary Sciences*, edited by Y. Syono and M. H. Manghnani, pp. 323–331, American Geophysical Union, Washington DC. *Geophysical Research Letters*, *16*, 425–428.

Iwamori, H. (1992), Degree of melting and source composition of Cenozoic basalts in southwestern Japan: evidence for mantle

upwelling by flux melting, *Journal of Geophysical Research*, *97*, 10983–10995.

Jacobsen, S. D. (2006), Effect of water on the equation of state of nominally anhydrous minerals, in *Water in Nominally Anhydrous Minerals*, edited by H. Keppler and J. R. Smyth, Mineralogical Society of America, Washington DC.

Karato, S. (2003), Mapping water content in Earth's upper mantle, in *Inside the Subduction Factory*, edited by J. E. Eiler, pp. 135–152, American Geophysical Union, Washington DC.

Karato, S. (2006a), Hydrogen-related defects and their influence on the electrical conductivity and plastic deformation of mantle minerals: A critical review, in *Earth's Deep Water Cycle*, edited by S. D. Jacobsen and S. van der Lee, American Geophysical Union, Washington DC.

Karato, S. (2006b), Microscopic models for the influence of hydrogen on physical and chemical properties of minerals, in *Superplume: Beyond Plate Tectonics*, edited by D. A. Yuen, et al., p. in press, Springer.

Karato, S. (2006c), Remote sensing of hydrogen in Earth's mantle, in *Deep Earth Water Circulation*, edited by H. Keppler and J. R. Smyth, Mineralogical Society of America, Whagington DC.

Kawamoto, T., and J. R. Holloway (1997), Melting temperature and partial melt chemistry of H_2O-saturated peridotite to 11 gigapascals, *Science*, *276*, 240–243.

Koga, K., et al. (2003), Hydrogen concentration and analyses using SIMS and FTIR: Comparison and calibration for nominally anhydrous minerals, *Geochem. Geophys. Geosyst.*, *4*, 10.1029/2002GC000378.

Kohlstedt, D. L., et al. (1996), Solubility of water in the α, β and γ phases of $(Mg,Fe)_2SiO_4$, *Contributions to Mineralogy and Petrology*, *123*, 345–357.

Lange, R. L., and I. S. E. Carmichael (1990), Thermodynamic properties of silicate liquids with emphasis on density, thermal expansion and compressibility, *Review of Mineralogy*, *24*, 25–64.

Leahy, G., and D. Bercovici (2004), The influence of the transition-zone water filter on convective circulation in the mantle, *Geophysical Research Letters*, *31*, 10.1029/2004GL021206.

Leahy, G., and D. Bercovici (2006), On the entrainment of hydrous melt above the transition zone, *Earth and Planetary Science Letters*, submitted.

Litasov, K., and E. Ohtani (2002), Phase relations and melt compositions in CMAS-pyrolite-H_2O system up to 25 GPa, *Physics of Earth and Planetary Interiors*, *134*, 105–127.

Lu, R., and H. Keppler (1997), Water solubility in pyrope to 100 kbar, *Contributions to Mineralogy and Petrology*, *129*, 35–42.

Matsukage, K. N., et al. (2005), Density of hydrous silicate melt at the conditions of the Earth's deep upper mantle, *Nature*, *438*, 488–491.

McDonough, W. F., and S.-S. Sun (1995), The composition of the Earth, *Chemical Geology*, *120*, 223–253.

McKenzie, D. (1984), The generation and compaction of partially molten rocks, *Journal of Petrology*, *25*, 713–765.

Mierdel, K., and H. Keppler (2004), The temperature dependence of water solubility in enstatite, *Contributions to Mineralogy and Petrology*, *148*, 305–311.

Miyashiro, A. (1986), Hot regions and the origin of marginal basins in the western Pacific, *Tectonophyiscs*, *122*, 195–216.

Newsom, H. E. (1995), Composition of the solar system, planets, meteorites, and major terrestrial reservoirs, in *Global Earth Physics: A Handbook of Physical Constants*, edited by T. H. Ahrens, pp. 159–189, American Geophysical Union, Washington DC.

O'Nions, R. K., and E. R. Oxburgh (1983), Heat and helium in the Earth, *Nature*, *306*, 429–431.

Obayashi, M., et al. (2006), High temperature anomalies oceanward of subducting slabs at the 410-km discontinuity, *Earth and Planetary Science Letters*.

Ohtani, E., et al. (2000), Stability of dense hydrous magnesium silicate phases in the system Mg_2SiO_4-H_2O and $MgSiO_3$-H_2O at pressures up to 27 GPa, *Physics and Chemistry of Minerals*, *27*, 533–544.

Ohtani, E., et al. (1995), Melting relations of peridotite and the density crossover in planetary mantles, *Chemical Geology*, *120*, 207–221.

Ohtani, E., et al. (2001), Stability of dense hydrous magnesium silicate phases and water storage capacity in the transition zone and lower mantle, *Physics of Earth and Planetary Interiors*, *124*, 105–117.

Parman, S. W., et al. (2005), Helium solubility in olivine and implications for high $^3He/^4He$ in ocean island basalts, *Nature*, *437*, 1140–1143.

Rauch, M., and H. Keppler (2002), Water solubility in orthopyroxene, *Contributions to Mineralogy and Petrology*, *143*, 525–536.

Revenaugh, J., and S. A. Sipkin (1994), Seismic evidence for silicate melt atop the 410-km mantle discontinuity, *Nature*, *369*, 474–476.

Richard, G., et al. (2006b), Slab dehydration in the Earth's mantle transition zone, *Earth and Planetary Science Letters*, in press.

Richard, G., et al. (2006a), Slab dehydration and fluid migration at the base of the upper mantle: implication for deep earthquake mechanisms, *Geophysical Journal International*, in press.

Richard, G., et al. (2002), Is the transition zone an empty water reservoir? Inference from numerical model of mantle dynamics, *Earth and Planetary Science Letters*, *205*, 37–51.

Sakamaki, T., et al. (2006), Stability of hydrous melt at the bottom of the Earth's upper mantle, *Nature*, *439*, 192–194.

Sneeringer, M., et al. (1984), Strontium and samarium diffusion in diopside, *Geochimica et Cosmochimica Acta*, *48*, 1589–1608.

Song, T.-R. A., et al. (2004), Low-velocity zone atop the 410-km seismic discontinuity in the northwestern United States, *Nature*, *427*, 530–533.

Spiegelman, M., and T. Elliott (1993), Consequences of melt transport for uranium series disequilibrium in young lavas, *Earth and Planetary Science Letters*, *118*, 1–20.

Stalder, R., et al. (2001), High pressure fluids in the system MgO-SiO_2-H_2O under upper mantle conditions, *Contributions to Mineralogy and Petrology*, *140*, 607–618.

Suetsugu, D., et al. (2006), A study of temperature anomalies and water contents in the mantle transition zone beneath subduction zones as inferred from P-wave velocities and mantle discontinuity depths, in *Earth's Deep Water Cycle*, edited by S. van der Lee and S. D. Jacobsen, American Geophysical Union, Washington DC.

Takahashi, E. (1986), Melting of a dry peridotite KBL-1 up to14 GPa: implications on the origin of peridotitic upper mantle, *Journal of Geophysical Research*, *91*, 9367–9382.

Taura, H., et al. (1998), Pressure dependence on partition coefficients for trace elements between olivine and coexisting melts, *Physics and Chemistry of Minerals*, *25*, 469–484.

van der Hilst, R. D., et al. (1997), Evidence for deep mantle circulation from global tomography, *Nature*, *386*, 578–584.

van der Meijde, M., et al. (2003), Seismic evidence for water deep in Earth's upper mantle, *Science*, *300*, 1556–1558.

van Keken, P. E., et al. (2002), Mantle mixing: the generation, preservation, and destruction of chemical heterogeneity, *Annual Review of Earth and Planetary Sciences*, *30*, 493–525.

Van Orman, J. A., et al. (1998), Uranium and thorium diffusion in diopside, *Earth and Planetary Science Letters*, *160*, 505–519.

Wang, W., and E. Takahashi (2000), Subsolidus and melting experiments of K-doped peridotite KLB-1 to 27 GPa; Its geophysical and geochemical implications, *Journal of Geophysical Research*, *105*, 2855–2868.

Withers, A. C., et al. (1998), The OH content of pyrope at high pressure, *Chemical Geology*, *147*, 161–171.

Wolfe, C. J., and P. G. Silver (1998), Seismic anisotropy of oceanic upper mantle: shear wave splitting methodologies and observations, *Journal of Geophysical Research*, *103*, 749–771.

Wood, B. J. (1995), The effect of H_2O on the 410-kilometer seismic discontinuity, *Science*, *268*, 74–76.

Wood, B. J., and J. D. Blundy (2002), The effect of H_2O on crystal-melt partitioning of trace elements, *Geochimica et Cosmochimica Acta*, *66*, 3647–3656.

Yoshino, T., et al. (2006), Complete wetting of olivine grain-boundaries by a hydrous melt near the mantle transition zone, *Earth and Planetary Science Letters*, submitted.

Young, T. E., et al. (1993), Infrared spectroscopic investigation of hydroxyl in β-$(Mg,Fe)_2SiO_4$ and coexisting olivine: implications for mantle evolution and dynamics, *Physics and Chemistry of Minerals*, *19*, 409–422.

Zhao, D. (2004), Global tomographic images of mantle plumes and subducting slabs: insights into deep mantle dynamics, *Physics of the Earth and Planetary Interiors*, *146*, 3–34.

Zhao, Y.-H., et al. (2004), Solubility of hydrogen in olivine: dependence on temperature and iron content, *Contributions to Mineralogy and Petrology*, *147*, 155–161.